



**HAL**  
open science

## Luminescent lanthanide nanoparticle-based imaging enables ultra-sensitive, quantitative and multiplexed in vitro lateral flow immunoassays

F. Mousseau, C. Féraudet Tarris, S. Simon, T. Gacoin, A. Alexandrou, C I Bouzigues

### ► To cite this version:

F. Mousseau, C. Féraudet Tarris, S. Simon, T. Gacoin, A. Alexandrou, et al.. Luminescent lanthanide nanoparticle-based imaging enables ultra-sensitive, quantitative and multiplexed in vitro lateral flow immunoassays. *Nanoscale*, 2021, 13 (35), pp.14814 - 14824. 10.1039/d1nr03358a . hal-03878185

**HAL Id: hal-03878185**

**<https://hal.science/hal-03878185>**

Submitted on 29 Nov 2022

**HAL** is a multi-disciplinary open access archive for the deposit and dissemination of scientific research documents, whether they are published or not. The documents may come from teaching and research institutions in France or abroad, or from public or private research centers.

L'archive ouverte pluridisciplinaire **HAL**, est destinée au dépôt et à la diffusion de documents scientifiques de niveau recherche, publiés ou non, émanant des établissements d'enseignement et de recherche français ou étrangers, des laboratoires publics ou privés.

# Luminescent lanthanide nanoparticle-based imaging enables ultra-sensitive, quantitative and multiplexed *in vitro* Lateral Flow Immunoassays

F. Mousseau<sup>a\*</sup>, C. Féraudet Tarrisse<sup>b</sup>, S. Simon<sup>b</sup>, T. Gacoin<sup>c</sup>, A. Alexandrou<sup>a‡</sup> and C. I. Bouzigues<sup>a‡</sup>

<sup>a</sup> Laboratoire d'Optique et Biosciences, Ecole Polytechnique, Institut Polytechnique de Paris, CNRS, INSERM, Route de Saclay, 91128 Palaiseau, France.

<sup>b</sup> Université Paris-Saclay, CEA, INRAE, Département Médicaments et Technologies pour la Santé (DMTS), 91191 Gif-sur-Yvette, France.

<sup>c</sup> Laboratoire de Physique de la Matière Condensée, Ecole Polytechnique, Institut Polytechnique de Paris, CNRS, Route de Saclay, 91128 Palaiseau, France

## ABSTRACT

Lateral Flow Assays (LFAs) have been extensively used on-site to rapidly detect analytes, possibly in complex media. However, standard gold nanoparticle-based LFAs lack sensitivity and cannot provide quantitative measurements with high accuracy. To overcome these limitations, we image lanthanide-doped nanoparticles (YVO<sub>4</sub>:Eu 40%) as new luminescent LFA probes, using a homemade reader coupled to a smartphone and propose an original image analysis allowing strip quantification regardless of the shape of the test band signal. This method is demonstrated for the detection of staphylococcal enterotoxins SEA, SEG, SEH, and SEI. A systematic comparison to state-of-the-art gold nanoparticle-based LFA revealed an analytical sensitivity enhancement of at least one order of magnitude. We furthermore provided measurements of absolute toxin concentration over two orders of magnitude and demonstrated simultaneous quantitative detection of multiple toxins with unaltered sensitivity. In particular, we reached concentrations 100 times lower than the ones reported in the literature for on-site multiplexed LFA targeting enterotoxins. Altogether, these results highlight that our luminescent nanoparticle-based method provides

a powerful and versatile on-site framework to detect multiple biomolecules with sensitivity approaching that obtained by ELISA. This paves the way to a change of paradigm in the field of analytical immunoassays by providing fast *in situ* quantitative high sensitivity detection of biomarkers or pathogens.

**Key words:** Lateral Flow Assay (LFA), europium-doped nanoparticles, luminescent particles, gold nanoparticles, staphylococcal enterotoxin, multiplex.

## INTRODUCTION

The on-site detection of biomarkers and pathogens is indispensable for resource-constrained areas. In this context, the World Health Organization established the ASSURED criteria (Affordable, Sensitive, Specific, User-friendly, Rapid and robust, Equipment-free and Deliverable to end-users) to identify the most appropriate diagnostic tests<sup>1</sup>. However, assays performed on-site are usually not sensitive enough and only semi-quantitative.

The Lateral Flow Assay (LFA), also known as immunochromatographic strip, is a powerful membrane-based platform used to detect targeted analytes in complex samples within 5 – 30 min (Figure 1a). It has gained interest in many areas (like point-of-care diagnostics, food safety, drug testing, forensic analysis, environmental monitoring) because of its simplicity, rapidity, specificity, portability and user-friendly format<sup>2,3</sup>, making it the only rapid diagnostic assay that meets most of the ASSURED criteria<sup>1</sup>. Examples of consumer use are pregnancy tests sold in pharmacies and antigen tests for the detection of COVID-19. In LFA, the sample flows along the membrane by capillarity (Figure 1a and b). In a format designed for a single analyte detection, a positive sample is indicated by the appearance of two lines (test and control) while only one line (control) is observed for a negative one.

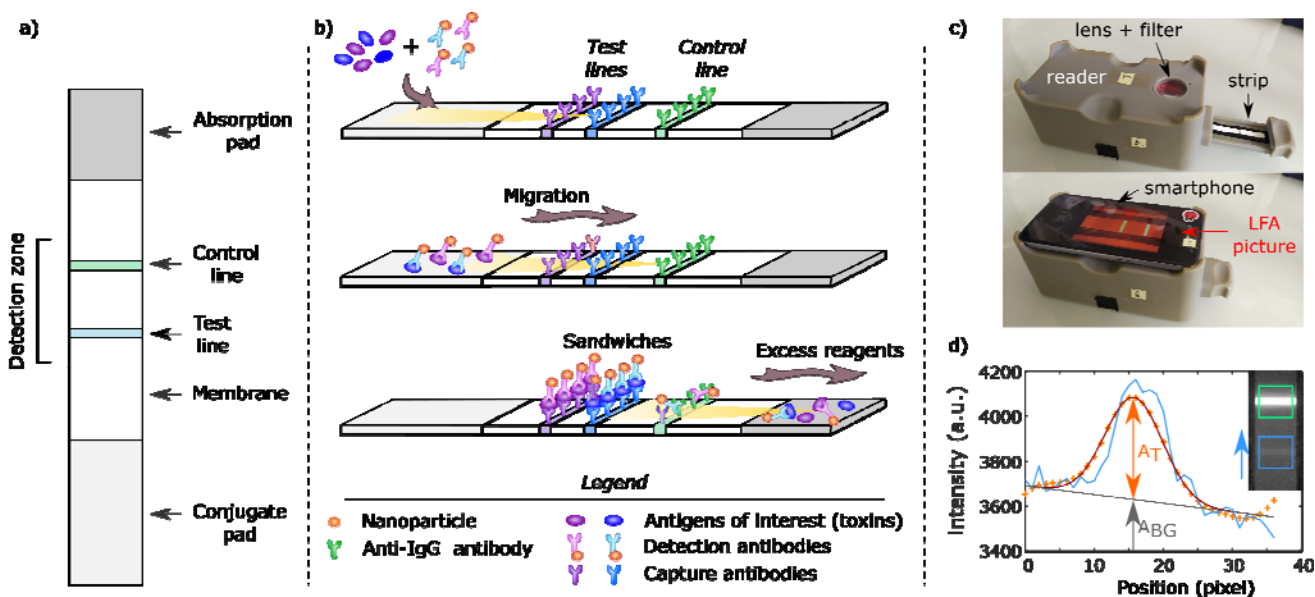


Figure 1 : a) Strip constitution for a simplex assay. b) Principle of a multiplexed LFA run in a dipstick format (the process is similar for simplex LFA but with only one toxin, one test line and one type of labeled NP). During sample migration along the strip, if the antigen of interest (toxin) is present, it first interacts with the detection antibodies labeled by a reporter. The obtained complexes then migrate along the strip and interact with the capture antibodies deposited onto the test line. Finally, the sample and the particles flow through the control line, consisting of a secondary antibody which captures the remaining reporter-labeled antibodies. c) Portable reader coupled to a smartphone for the LFA image capture. d) LFA quantitative analysis (example of a strip labeled with europium-doped NPs). The raw data are in blue (signal profile averaged along the width of the strip as a function of the position across the test line inside the Region Of Interest (ROI) also shown in blue in the strip image), the data convoluted by a Gaussian function are in orange and the Gaussian fit of the convoluted data and the background are in red and grey respectively.  $A_T$  and  $A_{BG}$  represent the amplitudes of the test line and the background respectively. The inset illustrates the position of the green and blue ROIs around the control and test lines respectively on the corresponding strip.

Gold nanoparticles (Au NPs) are the most common reporters used in LFAs due to their low production cost, stability, and simple read-out<sup>4</sup> (observation of a reddish colour due to the surface plasmon resonance phenomenon<sup>5</sup>). They however present several limitations. In particular, they have a low analytical sensitivity compared to the laboratory-based techniques like ELISA or LC-MS<sup>4</sup>, except when sophisticated

gold-based nanomaterials are used<sup>6</sup>. Second, even if this is not an inherent limitation of gold NPs but rather the price to pay for ease of use, strips are usually analyzed by naked-eye inspection, providing a user dependent “yes/no” result<sup>7</sup>.

Different strategies have been explored to improve LFA test sensitivity by using novel revelation methods or by enhancing the read-out process. In particular, alternative luminescent nanomaterial reporters have been explored such as quantum dots and silica or polymeric nanoparticles doped by organic dyes<sup>2-4</sup>. The advantage of fluorescence-based assays is that the signal is detected in almost background-free conditions. However, organic dyes photobleach while quantum dots are complex to transfer to aqueous solvents and to functionalize and present blinking and colloidal stability issues<sup>2</sup>. In this context, lanthanide-ion based reporters have been identified as promising luminescent probes because of their remarkable optical properties (narrow photoluminescence spectra, large Stokes shift, absence of blinking or photobleaching, high effective absorption cross section in the UV for certain matrix materials like YVO<sub>4</sub> and long luminescence lifetime)<sup>4,8</sup>. First, chelates of lanthanide ions were considered. Since each chelate contains only a single luminescent ion, it constrains *de facto* the achievable sensitivity by limiting the emitting ion number per targeted molecule. Second, chelates of lanthanide ions were embedded in organic (*e.g.* latex) or inorganic (*e.g.* silica) nanoparticles. Although this provides significant increase in emission signals and thus in LFA sensitivity<sup>9,10</sup>, the maximum number of lanthanide ions per nanoparticle is limited by the size of the organic chelator (between 0.02 and 0.3 lanthanide ions per nm<sup>3</sup> of nanoparticle volume as calculated from literature data)<sup>9,11,12</sup> and/or by the complexity of the reporter synthesis<sup>10,11</sup>. Third, up-conversion nanoparticles, which can emit visible light when irradiated in the infra-red (IR) and diminish autofluorescence, were shown to improve the sensitivity by one to two orders of magnitude when used in LFA<sup>2,13,14</sup>. However, their excitation requires powerful laser diodes and focusing - rendering multiplexing more complex - to compensate their low quantum yield<sup>4</sup>. Nevertheless, recent progress in near-IR lasers and in synthesis of higher quantum-yield materials of different emission colours<sup>15</sup> render this alternative promising.

Fourth, persistent luminescence nanoparticles, which are known to not require excitation at the same time as the detection, have been shown to improve LFA sensitivity<sup>16</sup>. Nevertheless, their phosphorescence lifetime on the time scale of minutes implies that long acquisitions (>10 min) are required to analyse a single strip, even though further recent optimizations allowed to reduce the reading time<sup>17,18</sup>. Meanwhile, the use of luminescent reporters implies the development of affordable and portable readers for luminescence excitation, detection and quantification, which is still an open issue<sup>10,19</sup>.

Instrument-based read out was developed to provide quantitative and objective signal interpretation of the data and to automatically archive and transmit the results<sup>6,20</sup>. Nevertheless, most commercial readers are expensive and can be used only in combination with the test systems from the same manufacturer, which substantially limits the scope of quantitative immunochromatography use<sup>20</sup>. For these reasons, numerous smartphone-based tools have been developed, in order to provide a LFA quantitative read-out and to objectively discriminate between positive and negative samples or implement quantitative detection<sup>20-22</sup>. A notable example is the use of a smartphone camera flash for excitation and of a simple and cheap smartphone adaptor for the rapid detection of persistent luminescence nanoparticle probes<sup>17,18</sup>. However, regardless of the reader type, analysis is thorny for strips labeled by Au NPs and subject to errors due to the time evolution of Au NPs based signals after LFA completion if the inspection is not performed during the time interval indicated by the manufacturer. Indeed, gold nanoparticles tend to aggregate on the test and control lines after their capture, leading to a shift of the plasmon resonance to longer wavelengths<sup>23</sup>. The LFA architecture is particularly suited to multiplexing since it enables the presence of more than one test line in a single device<sup>24,25</sup> (Figure 1b). However, the multiplexed LFAs (xLFAs) often lose sensitivity due to cross-reactivity<sup>24,26</sup>. In addition, visual interpretation becomes complicated when increasing the number of test lines, particularly in the case of low positive signals and high-throughput multiplexed assays, for which the use of a reader seems mandatory to provide reliable results<sup>24</sup>.

The rapid and portable detection of staphylococcal enterotoxins (SEs) in water or food matrices is of capital importance but has remained limited so far<sup>27</sup>. SEs, secreted by the pathogen *Staphylococcus aureus*, are thought to be responsible for numerous human diseases including foodborne illnesses (one of the world's leading health issues), sepsis-related infections, toxic shock syndrome and immune system failures<sup>28</sup>. In addition, SEs are resistant to denaturing conditions, such as low pH, high temperatures and proteolytic digestion, toxic at minute quantities, making them potential biological weapons<sup>28</sup>. Numerous techniques like liquid chromatography coupled to mass spectroscopy (LC-MS), immunoassays (ex: ELISA), surface plasmon resonance (SPR), surface-enhanced Raman spectroscopy (SERS) and quartz crystal microbalance assays (QCM) have been employed to detect SEs<sup>27</sup>. Despite their sensitivity and specificity, the cost and time to obtain the results and the requirement for specific lab equipment and trained operators limit drastically their use in the field<sup>27</sup>.

In this work, we propose, as new highly efficient LFA probes, metal oxide nanoparticles YVO<sub>4</sub>:Eu (40%), where lanthanide ions (Eu<sup>3+</sup>) directly replace the Y<sup>3+</sup> ions in the crystalline matrix, allowing a high doping rate by luminescent ions to overcome current limitations (12 Eu<sup>3+</sup> per nm<sup>3</sup>, that is 40 to 600 times more than what is described in the literature for nanoparticles doped with europium chelates). Thanks to their excellent optical properties and low cytotoxicity, we previously demonstrated that our europium-doped nanoparticles (Eu NPs) could be efficiently detected at the single particle level with a standard epifluorescence microscope in different biological environments for various applications<sup>29-32</sup>.

We used these novel LFA probes to detect four of the SEs toxins (SEA, SEG, SEH and SEI). Strips were then analyzed by a homemade portable reader coupled to a smartphone. Our system enables the robust and quantitative detection of all four SEs for concentrations of few pg.mL<sup>-1</sup>, demonstrating a substantial sensitivity gain (1-2 orders of magnitude) compared to the gold NP-detection standard. Finally, we devised a multiplexed assay in which three enterotoxins were detected with a 100 sensitivity enhancement<sup>33</sup>,

thus approaching or surpassing the ELISA sensitivity. Our system can be easily adapted to a vast range of analytes for on-site, fast, ultra-sensitive and versatile immunoassays.

## **MATERIAL AND METHODS**

### **Chemicals**

The origin of chemicals and salts is detailed in the Supplementary Information S1.1. All products were used without further purification. Water was deionized with a Millipore Milli-Q Water system (Merck).

### **Materials**

*Antibodies and antigens.* To date, 19 different Staphylococcal Enterotoxins (SEs) have been shown to induce staphylococcal food poisoning<sup>34</sup>. We selected for this work the toxin SEA because it is the most common SE toxin involved in foodborne illnesses<sup>34</sup>. In addition, we considered the toxins SEG, SEH, and SEI because they are less studied since their discovery is more recent while they are probably as dangerous as the other SEs<sup>34</sup>.

Monoclonal antibodies (Abs) were raised in Biozzi mice by immunization with recombinant staphylococcal enterotoxins SEA (molecular weight  $M_w = 28.3$  kDa), SEG ( $M_w = 28.2$  kDa), SEH ( $M_w = 26.3$  kDa) or SEI ( $M_w = 26.1$  kDa) that were expressed in *E. coli*, purified as detailed in S1.2<sup>34</sup> and fully characterized by bottom-up mass spectrometry<sup>35</sup>. Antibodies were produced, purified by protein A affinity chromatography and characterized as described in previous work (isotyping, kinetic parameters, complementarity binding study, use in ELISA and LFA immunoassays)<sup>34</sup>.

*Nanoparticles.* Spherical gold nanoparticles of 41 nm, which is in the classical NP size range considered in LFA, were purchased from BBI Solution (reference HD.GC40.OD10). The  $YVO_4:Eu$  (40 %) NPs were

synthesized by salt co-precipitation and silicated, aminated and finally carboxylated as described in our previous work<sup>36-39</sup> and in Supplementary Information S2.1. In our conditions, 40 % of  $Y^{3+}$  ions constituting the  $YVO_4$  matrix are replaced by luminescent  $Eu^{3+}$  ions. Both Au and Eu NPs were then characterized (S2.2) and coupled to the detection antibodies (S2.3). Antibodies were covalently attached onto Eu NPs with a targeted Ab:NP molar ratio of 20, whereas they passively adsorbed on Au NPs, consuming therefore much more antibodies while they represent the most expensive contribution to the LFA assay cost. Nanoparticle characteristics are summarized in Table 1.

|                               | Au NP | Eu NP       |
|-------------------------------|-------|-------------|
| $D_0$ (nm)                    | 40.8  | 12.0 / 26.3 |
| $D_H$ (nm)                    | 41    | 130         |
| Plasmon resonance (nm)        | 526   | /           |
| Quantum yield (%)             | /     | 4.8         |
| $\lambda_{ex}$ (nm)           | /     | 280         |
| $\lambda_{em}$ (nm)           | /     | 617         |
| Ab ( $\mu$ g per pmol of NPs) | 90    | 3           |

Table 1 : Nanoparticle characteristics: geometric ( $D_0$ ) and hydrodynamic ( $D_H$ ) diameters determined by transmission electron microscopy and dynamic light scattering respectively, plasmon resonance of the Au NPs, quantum yield, excitation ( $\lambda_{ex}$ ) and emission ( $\lambda_{em}$ ) wavelength of the Eu NPs and amount of antibodies used to functionalize 1 pmol of NPs. In the case of Eu NPs,  $D_H$  is significantly larger than  $D_0$ , which is due to the oblong shape of the particles and their polydispersity, the DLS measurement strongly overestimating the contribution of larger particle sizes.

## Methods

*Strip assembly.* The test and control lines were printed with capture antibodies (prepared as described in Materials) and goat anti-mouse IgG (Ab6708, Abcam) antibody, at concentrations of 1 and 0.5  $mg \cdot mL^{-1}$  respectively ( $1 \mu L \cdot cm^{-1}$ ,  $50 mm \cdot s^{-1}$ ) with a Frontline<sup>TM</sup> microliter contact dispenser (BioDot, USA) onto a FF120HP nitrocellulose membrane (Whatman<sup>TM</sup>, GE Healthcare Europe, Germany). Membranes were then treated to avoid non-specific signals<sup>40</sup>, assembled and cut as described in S3.1. The xLFIA strips were obtained by printing 3 test lines and one control line along the nitrocellulose membrane as this

technique requires minimum manipulation of the assay architecture (Figure 1b)<sup>24</sup>. Membranes were then treated, assembled and cut with the same protocol as the one designed for the simplex assay. Since the time of interaction between species is short in LFA, the assay sensitivity in multiplexed tests may depend on the test line position along the strip. For each of the 3 toxins considered here, the signal was thus observed as a function of the test line position and showed no dependence on this parameter (see S3.2). To limit the non-specific detection of the toxin SEH by the capture antibodies targeting SEG (see the “Results and Discussion” section), the order of the multiplexed test lines is chosen so that the sample first meets the test line recognizing the toxin SEH, then the one detecting the toxin SEG.

*LFA procedure (dipstick format)*. 100  $\mu$ L of sample (NPs and toxins) in a migration solution (0.1 % BSA, 0.5 % Tween 20, 0.01 % azide, 150 mM NaCl in a potassium phosphate buffer – 100 mM, pH 7.4) were prepared in wells of a 96-well plate. The strips were dipped into the solution immediately after preparation for 25 min (see S3.3). The indicated toxin and nanoparticle concentrations refer to the final concentration in the 100  $\mu$ L dispersions. The number of nanoparticles used per LFA strip was previously optimized (data not shown). Briefly, the highest NP concentration inducing no signal on the test line for a sample in the absence of toxin was selected for strips labeled with gold nanoparticles. The highest NP concentration common to the four toxins inducing no or low non-specific signal on the test line for samples containing no toxin was chosen for labeling with Eu NPs. Data are summarized in Table 2 and show that approximately 12 times less detection antibodies are required to perform an assay with the Eu NPs.

|      |                                | Au NP | Eu NP |
|------|--------------------------------|-------|-------|
| LFA  | NP per strip ( $\times 10^9$ ) | 6.7   | 17.2  |
|      | Capture Ab per strip (ng)      | 997   | 85    |
| xLFA | NP per strip ( $\times 10^9$ ) | /     | 8.6   |
|      | Capture Ab per strip (ng)      | /     | 43    |

Table 2 : Number of nanoparticles and amount of capture antibodies used in a single LFA run per toxin for Au and Eu NPs. The global NP and Ab quantities per strip for the multiplexed assay are 3 times higher than the values indicated in the table, as 3 toxins are simultaneously detected on the strip.

*Lateral flow reader, image collection and image processing.* LFA strips were imaged through the smartphone camera in the minute following the run completion, the time between the start of sample migration and the strip imaging having to be constant in the case of strips labeled with Au NPs to avoid changes in the test and control line colour. Images were acquired with a smartphone Samsung Galaxy S7 coupled to a portable reader designed and fabricated by Bitmakers (Fontains, France) based on a home-made prototype. The reader enabled a dual illumination in the visible range (with 2 white light LEDs) and in the UV (with 20 LEDs of 2 mW at 278 nm, LEUVK37B50HF00, Laser Components) for the Au and Eu NPs respectively. The LED disposition inside the reader, which is displayed in S4, results in a typical low intensity of  $4 \text{ mW.cm}^{-2}$ . This leads to an important reduction of excitation signal leaks and consequently of the overall parasite signals in comparison to powerful excitation sources. Additionally, a red filter was added in the optical path for Eu-doped nanoparticle observation to eliminate background signal and thus increase the signal-to-noise ratio.

Eu NPs used for live cell labeling have previously been excited by a laser in the visible range (466 nm, direct excitation of the  $\text{Eu}^{3+}$  ions) to avoid phototoxicity<sup>29,30,41</sup>. However, for *in vitro* applications, europium can be excited in the UV where the vanadate ion absorption cross section is much higher (280 nm, excitation of the vanadate ions followed by energy transfer to the europium ion<sup>37</sup>), which has enabled the development of a simple and small LED-based reader. A smartphone application has been coded to photograph the strips with fixed capture parameters (exposure time, focus, gain) and save them on the smartphone (Figure 1c). In these conditions, there are negligible variations of the strip position and orientation and the lighting conditions were reproducible from one strip readout to another, which is important to perform reliable quantitative analysis.

Image analysis was performed in Matlab without any contrast enhancement or brightening of the images. Briefly, the operator indicates to the algorithm an approximate initial position of the control line. The

distance between the test and control lines being known, an approached position of the test line is automatically determined. In order to guarantee the highest robustness in the image processing analysis, Regions Of Interest (ROIs) large but smaller than the strip width<sup>7,17</sup> are defined around each initial position (see inset of Figure 1d). The count values of the RGB images are averaged for the pixels along the small axis of the strip width, inverted in the case of Au-labeled assays, and convoluted with a normalized Gaussian (whose width is larger than that of the test line) to obtain a smoothed profile of the strip, giving thus a standard, *i.e.* independent of the actual band shape, profile without modifying the integral of the signal intensity. The convoluted test and control line profiles were then fitted with a Gaussian on top of a background displaying a linear slope, as displayed in Figure 1d (see S5 for more examples). In the case of gold labels, the final signal was defined as the ratio of the amplitudes of the test and control fits, as usually reported in the literature. However, when the Eu NPs were used, the control line was saturated, thus preventing correcting for any possible excitation intensity variations. To circumvent this difficulty, the final signal was calculated as the ratio of the test line amplitude over the background (Figure 1d).

Concerning the xLFA quantification, the operator still indicates to the algorithm the approximate position of the control line, enabling the placement of ROIs around the three test lines since their spacing is known. The same procedure as the one developed for the simplex analysis is then used.

## RESULTS AND DISCUSSION

To demonstrate the efficiency of europium-doped nanoparticles (Eu NPs) as LFA probes, we first perform comparative LFA tests using gold nanoparticles (Au NPs) and Eu NPs with identical pairs of capture and detection antibodies, the latter being passively adsorbed on the Au NP surface (Ab:NP molar ratio of 600 in the labeling solution) and covalently bound to the Eu NPs (Ab:NP molar ratio of 20). Figure 2 displays the strips obtained in the presence of varying SEH toxin concentrations. By naked-eye observation, we estimate the approximate lowest visible concentration (LVC) to be around 500 and 50  $\text{pg}\cdot\text{mL}^{-1}$  with Au

and Eu NPs, respectively. Similar results are obtained for the three other toxins SEA, SEG and SEI (see S6) where gains of approximately 5, 10, and 10 are respectively observed with Eu NPs (results are summarized in Table 3). We thus obtained a significantly enhanced analytical sensitivity compared to the gold reference by using the standard qualitative naked-eye readout method.

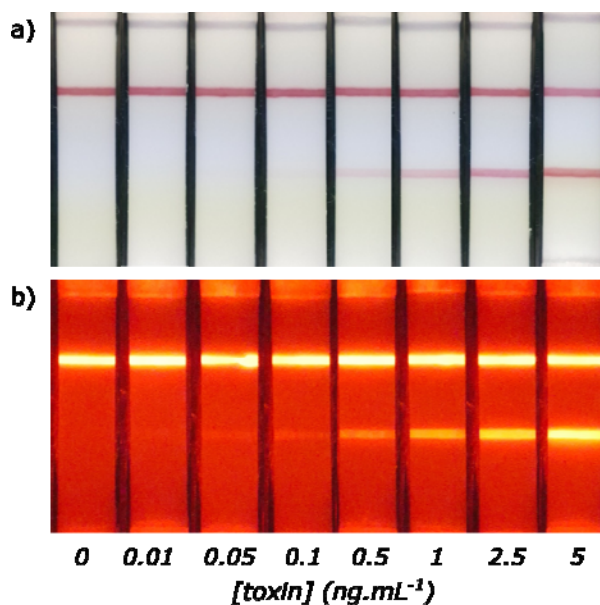


Figure 2 : LFA strips labeled with gold (a) and europium-doped (b) nanoparticles for the detection of the SEH toxin (concentrations ranging from 10 pg.mL<sup>-1</sup> to 5 ng.mL<sup>-1</sup>). Note that all strip images presented in our work were taken with the smartphone camera. The strips are illuminated with white light LEDs and UVs LEDs respectively when labeled with Au and Eu NPs. The red background displayed by strips run with europium-doped nanoparticles is not due to the autofluorescence of the strip or the buffer but mainly to the luminescence of NPs non-specifically adsorbed on the nitrocellulose membrane (see SI 8).

The origin of this enhanced sensitivity is twofold: i) It is generally advantageous to detect an emission signal (e.g. the fluorescence of the Eu NPs) rather than an absorption signal (e.g. the red colour of the Au NPs due to the absorption in the blue by their surface plasmon). Indeed, an absorption signal is always detected on top of a bright background. The signal-to-noise ratio is determined by the noise related to the

presence of this bright background. In contrast, an emission signal is theoretically detected in the presence of a dark background, the noise being only related to the inherent fluctuations of the signal itself. In practice, in LFA tests, there is usually a non-specific contribution from the background, much weaker than the one observed in an absorption experiment, which gives rise to the related noise fluctuations. Therefore, detection of an emission signal rather than an absorption one of similar amplitude leads to improved sensitivity. ii) The excellent absorption and emission properties of the Eu-doped nanoparticles (narrow photoluminescence spectra, large Stokes shift, absence of blinking or photobleaching, and good quantum yield) translate into collection of high numbers of photons well separated spectrally from the excitation ones. In contrast to our previous work on living cells where direct  $\text{Eu}^{3+}$  excitation in the visible was used<sup>29-32</sup>, we here exploit the strong absorption of the vanadate ions of the matrix which absorb in the UV with a maximum at 280 nm ( $\epsilon \approx 4\,000\text{ M}^{-1}\cdot\text{cm}^{-1}$ )<sup>42</sup> and the subsequent energy transfer of the excitation to the  $\text{Eu}^{3+}$  ions which emit at 617 nm (see Figure S2.3c). Thus, the absorption coefficient of our nanoparticles at 280 nm can be estimated to be  $1.7 \times 10^6\text{ M}^{-1}\cdot\text{cm}^{-1}$  based on the number of vanadate ions present in the crystalline matrix. This allows the use of low intensity UV LEDs as excitation source and cheap and compact power supply.

In order to study the variability inherent to the strip preparation, assays are then carried out in independent triplicates (*i.e.* on 3 different days) for the SEH, SEG and SEI toxins. The first two replicates are performed with a first batch of strips and the third one with a second batch obtained from the same nitrocellulose membrane, sample pad, absorption pad and antibody stocks. As displayed in S7 for SEH, a satisfactory reproducibility in the absolute test line intensity is observed for LFAs carried out on strips of the same batch. In contrast, we observed a significant interbatch variability, yet the overall assay sensitivity remained unchanged. This observation points to the requirement to perform a calibration (see below) for each batch before performing quantitative assays of any unknown sample.

In the qualitative Au NP-based LFA assays, it is crucial that there is no non-specific signal on the test line so that a readout with the naked eye is reliable. When a quantitative readout is possible, however, as this is the case with our approach, the presence of reporters non-specifically bound to the test line in the absence of toxin is not an issue. Indeed, the limit of detection can be calculated from the signal in the absence of analyte, as discussed below, to yield the lowest signal indicative of a non-zero concentration of analyte with a defined degree of certainty.

In addition, by comparing LFA performed in the absence or presence of Eu NPs, we demonstrate that reporters non-specifically bound to the nitrocellulose all along the membrane can be detected even in the absence of toxin (see S8), even in optimized conditions, *i.e.* with no detectable signal at the test line location. The substrate autofluorescence is thus not a limiting factor for our luminescence-based LFA sensitivity. Indeed, the sensitivity is not limited by the minimal number of detectable probes but by the residual signal due to the non-specific adsorption of NP-Ab conjugates along the strip, and more specifically on the test line. Therefore, further sensitivity enhancement would rely on biochemical optimization to reduce non-specific interactions.

We next define a framework to accurately compare the different LFA methods of analysis. Usually, quantitative immunoassays are characterized by their limit of detection (LOD) or by their limit of blank (LOB), which are defined by  $LOD = mean_0 + 3SD_0$  and  $LOB = mean_0 + 1.645 SD_0$  where  $mean_0$  and  $SD_0$  are the respective mean signal and standard deviation of the blanks (*i.e.* of the samples with no analyte)<sup>43</sup>. The signal value corresponding to the LOD (respectively LOB) sets the concentration above which (respectively below which) a sample has 99.7 % chances (respectively 90 %) of being truly positive (respectively truly negative). In qualitative conventional gold-based LFA, the sensitivity determined by visual inspection is characterized by a cut-off value, *i.e.* by the analyte concentration for which 50 % of the strips displayed an observable test line. This value can be considered as a qualitative analogue of the LOB. In our experiment, it is expected to lie between the analyte concentration of the last strip exhibiting only the

control line and the LVC. By considering all these definitions, we therefore retain LVC and LOB to reliably compare the qualitative and quantitative approaches with each other.

We then detect the luminescence signal of samples run in independent duplicates (on two different days but using the same strip batch). Their quantification, displayed in Figure 3, is obtained by an image analysis procedure that we developed and described in detail in the Material and Methods section. The point to be emphasized here is that our algorithm works for all profile shapes of test strip signals. In addition, blanks are run in 8 replicates over 8 different days, giving rise to the “zero” signal and enabling the calculation of the LOB. The signal obtained for concentrations roughly below  $50 \text{ pg.mL}^{-1}$  is initially lower than the LOB signal value and rises linearly when the toxin concentration increases<sup>6</sup>. For the SEG toxin, the signal variation is linear over the entire concentration range while it becomes sublinear at high toxin concentrations for SEA, SEH, and SEI<sup>6</sup>. As these signals do not saturate, quantitative detection can be achieved by fitting the data over the whole explored concentration range with a non-linear fit (see S9).

As illustrated in Figure 3b and S9, the fit of the signals from the calibration samples constitutes an efficient method to measure the absolute concentration of an unknown sample. Except for the SEA detection, which exhibits low sensitivity, the Eu NPs thus enable toxin quantification over two orders of magnitude of concentration, which represents an important advance for in-field applications<sup>10</sup>.

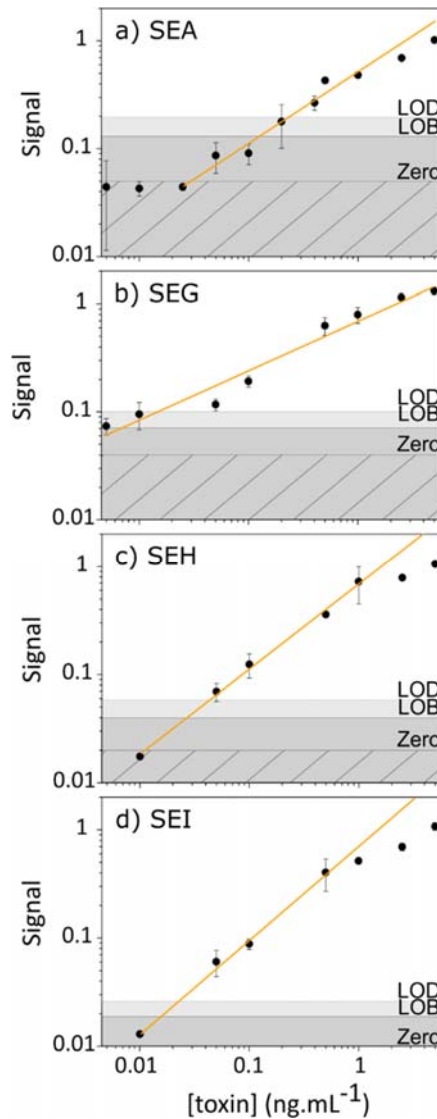


Figure 3 : Quantitative analysis of the SEA (a), SEG (b), SEH (c), and SEI (d) concentrations obtained with Eu-doped NPs as probes (errors bars indicate the standard deviation of two independent replicates). The zero, LOB, and LOD are calculated from 8 independent replicates performed in the absence of toxins by the following formulae:  $zero = mean_0$ ,  $LOB = mean_0 + 1.645 SD_0$  and  $LOD = mean_0 + 3 SD_0$ , where the mean value of the test line signals in absence of toxins is abbreviated  $mean_0$  and its standard deviation  $SD_0$ . The experimental data are fitted (orange curves) by  $\log(\text{Signal}) = A \cdot \log([\text{toxin}]) + B$ , the points at high concentrations not being taken into account when they lead to an increase of the coefficient  $R^2$ . The experimental points made for concentrations greater than or equal to 2.5, 2.5 and 1 ng.mL<sup>-1</sup> are not taken into account to establish the linear fit for the graphs a), c), and d) respectively. The constants A and B of the fits respectively equal 0.66 and -0.28 for SEA, 0.46 and -0.16 for SEG, 0.79 and -0.16 for SEH, and 0.87 and -0.14 for SEI.

With respective LOB values of 100, 7, 30 and 10  $\text{pg}\cdot\text{mL}^{-1}$  for the SEA, SEG, SEH, and SEI toxins (see Table 3), we obtain sensitivity gains of 18, 15, 18 and 38 compared to the reference assay (visual analysis of Au-labeled strips), as displayed in Figure 4. To identify the origin of the observed sensitivity gains, we quantitatively analyzed *via* our method the strips labeled with Au NPs (see S10 and Table 3) although this may not be relevant for on-site applications, as explained in the introduction. Based on these results, we first determine that our quantification through image analysis enhances the sensitivity compared to visual inspection for both NP types, which is in line with the literature<sup>10,20</sup>. However, the LOBs determined for all the toxins using Eu NP reporters are typically 10 times lower than the ones obtained with Au NPs, in agreement with the observations of the qualitative analysis (Figure 2 and S5). Our sensitivity gain thus relies on two effects: (i) on the thorough image analysis and (ii) on the optical efficiency of the Eu-doped NPs (see discussion above).

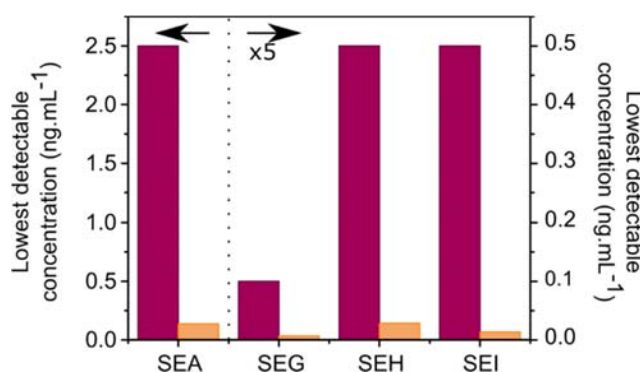


Figure 4 : Comparison of the lowest detectable concentration determined by visual inspection of the Au-labeled strips (LVC, purple bars) and by quantitative analysis of the Eu-labeled strips (LOB, orange bars). The left-y axis refers to SEA and the right one, which is magnified 5 times, refers to SEG, SEH and SEI.

By calculating LODs (see above and Table 3), we allow a quantitative comparison with the sensitivities obtained in our previous work in ELISA assays using the same pairs of antibodies in interaction with the same recombinant toxins<sup>34</sup> or in reference commercial enterotoxin detection tests. First, this comparison

indicates that our method using novel rare-earth-based-strips can detect toxin at concentrations approaching the ones that we previously reported through the *a priori* more sensitive ELISA assay<sup>34</sup>. Second, our luminescent LFA strips enable the detection of the toxins SEG, SEH, and SEI with LODs being respectively 17, 7, and 12 times lower than the one reached by Vidas SET 2 and RidaScreen SET Total, the two commercially available ELISA kit authorized by the European legislation for SEs detection in food matrices (LOD = 250 pg.mL<sup>-1</sup> according to user instructions<sup>44,45</sup>). This gain in sensitivity is partly due to the implementation of high-affinity antibodies<sup>34</sup> and partly due to our novel nanoparticle probes. Altogether, these elements points to the possibility to substitute conventional ELISA tests with fast and in-field deployable lanthanide-nanoparticle based LFA, without scarifying analytical sensitivity.

We then devise the multiplexed detection of the 3 toxins exhibiting the highest sensitivity gains in the simplex experiments (SEG, SEH, and SEI). In order to establish the feasibility of xLFA, we measure the possible cross-talks between the different toxin systems by testing all the “test line/toxin/Eu NPs” combinations in simplex LFA (abbreviated “SEX/SEY/SEZ”). For instance, a strip with a capture antibody specific to the toxin SEG is used to detect the toxin SEH with Eu NPs coated by SEI detection antibodies (SEG/SEH/SEI). The assays are carried out in the most unfavourable conditions, *i.e.* for the highest toxin concentration considered in this work (5 ng.mL<sup>-1</sup>) in the absence of the nanoparticles targeting the tested toxin. After quantitative analysis, all the detected signals (except for the reaction of the SEG/SEH/SEX systems) lie below the LOBs, indicating no significant cross-reactivity (see S11). In the case of SEG capture antibodies in the presence of the SEH toxin, the non-specific signal represents 20 % of the one obtained with the “SEG/SEG/SEG” system studied above for a toxin concentration of 5 ng.mL<sup>-1</sup>. From our calibration tables we can assume that the signal arising from the SEH toxin captured by the SEG test line would be at least 2 times lower than the LOB for [SEG] < 0.5 ng.mL<sup>-1</sup>, meaning that the cross-reactivity should therefore be negligible for any toxin cocktail at low concentrations.

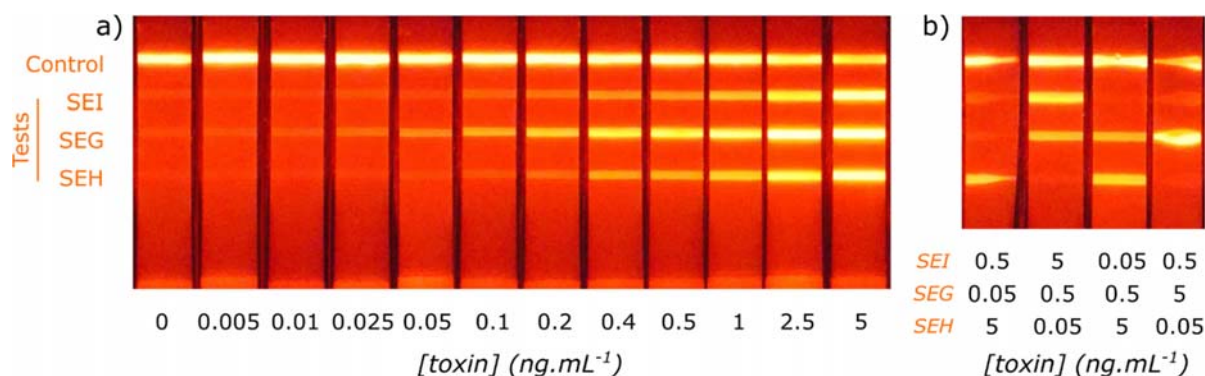


Figure 5 : xLFA strips labeled with europium-doped nanoparticles for the simultaneous detection of the SEG, SEH and SEI toxins at identical (a) or different (b) concentrations.

We first detect the toxins SEG, SEH and SEI spiked at the same concentrations (Figure 5a). The LOBs resulting from the quantification are, respectively, 20, 30, and 10  $\text{pg.mL}^{-1}$  for SEG, SEH, and SEI (see Figure S12 and Table 3), which is roughly 100 times lower than the reported detectable concentration for SEs detection in multiplexed LFA compatible with in-field use<sup>33</sup>. Furthermore, the xLFA performed with Eu NPs displays sensitivity gains of 5, 16 and 72 for SEG, SEH, and SEI, respectively, compared to non-multiplexed and visually read assays performed with Au NPs as reporters. The sensitivities are in the same range as the ones displayed by the simplex LFAs for the toxins SEH and SEI (Table 3). In contrast, we observe a loss in sensitivity for the SEG detection (Table 3) which is probably related to the cross-reactivity discussed above. We then compare these results to the calibration established through simplex experiments in Figure 3b and S9. It enables a rough estimate of the toxin concentrations, although the determination is not quantitative since a deviation factor of 0.9 to 2.9 from the nominal value is observed (see Table S12). Figure 5b shows xLFA strips for the 3 toxins at different concentrations in a single sample (see S13 for more examples). Concentrations are chosen at 0.05, 0.5 and 5  $\text{ng.mL}^{-1}$ , *i.e.* slightly above the LOBs, in the middle of the tested range, and at the highest concentration considered here. The toxin concentration being quantifiable with a bias of up to a factor of 3 in two thirds of the cases, this multiplex

assay thus enables a simultaneous and semi-quantitative determination of toxin concentrations. Nevertheless, a fully quantitative measurement in multiplex systems should be achievable by a calibration of all the accessible concentration combinations. Moreover, spectral multiplexing can be implemented in parallel with the spatial multiplexing by replacing the europium ions with lanthanide ions of different colors (such as Dy<sup>3+</sup>). This qualifies our system for fast, sensitive, and highly multiplexed quantitative detection.

|       |     | Au NPs |     |       | Eu NPs |     |      |     |      | ELISA            |                  |
|-------|-----|--------|-----|-------|--------|-----|------|-----|------|------------------|------------------|
|       |     | LVC    | LOB | LOD   | LVC    | LOB |      | LOD |      | LOD <sub>1</sub> | LOD <sub>2</sub> |
|       |     | LFA    | LFA | LFA   | LFA    | LFA | xLFA | LFA | xLFA |                  |                  |
| Toxin | SEA | 2 500  | 935 | 1 331 | 500    | 138 | /    | 240 | /    | 7                | 4                |
|       | SEG | 100    | 89  | 131   | 10     | 7   | 18   | 15  | 33   | 8                | 0.4              |
|       | SEH | 500    | 186 | 401   | 50     | 28  | 32   | 44  | 62   | 47               | 1                |
|       | SEI | 500    | 109 | 284   | 50     | 13  | 7    | 20  | 36   | 30               | 4                |

Table 3: Lowest visible concentration (LVC) obtained by subjective visual interpretation, and LOB and LOD calculated from quantitative analysis for LFA and xLFA, using Au and Eu NPs as reporters. We here show for comparison the LOD values obtained by ELISA in our previous work<sup>34</sup>. LOD<sub>1</sub> refers to the theoretical LOD determined under our screening conditions and with the same set of antibodies as the one used in this work (number of replicates n = 1). LOD<sub>2</sub> refers to the experimental LOD determined by optimized ELISA performed with the best couple of antibodies for this assay (number of replicates n = 20). Values are given in pg.mL<sup>-1</sup>.

## CONCLUSION

The detection of proteins like staphylococcal enterotoxins (SEs) lacks sensitive, quantitative and multiplexed on-site tools. In this work, we demonstrated that these issues can be addressed by using lanthanide-ion-based nanoparticles as a new class of LFA and xLFA reporters in association with a reader coupled to a smartphone. We report a significant decrease in the limit of detection of quantitative simplex and semi-quantitative multiplexed assays compared to the gold simplex standard. The LOD approaches or surpasses the sensitivity of the ELISA test that is the reference assay in laboratories. Strikingly, these performances are reached without adding cost and complexity or losing portability, which could hinder on-site LFA

deployment. Further analytical sensitivity enhancement could be obtained by increasing the effective affinity of the detection antibodies or by finely tuning the nanoparticle size or the Ab-to-NP ratio<sup>6,46</sup>. Our work thus opens new perspectives in point-of-care diagnostics in resource-constrained areas as it fully respects the ASSURED criteria identified by the WHO.

Our work can be easily transposed to other analytes and other LFA formats. Future developments for on-site detection will require i) performing the test with horizontal migration in a cassette, with sprayed nanoparticles on the conjugate pad instead of the dipstick format used here both for simplex and multiplexed strips and ii) optimization to detect analytes in real matrices instead of model buffers. Although performing the test in a horizontal cassette format typically leads to a sensitivity decrease due to a shorter reaction time between analyte and nanoparticle-labeled detection antibodies, we expect this effect to reduce the sensitivity of both Eu and Au-nanoparticle-based tests in a similar manner. Similarly, even though detecting analytes in real samples instead of in model buffers usually results in a loss of sensitivity, probably due to a passivation effect induced by the proteins naturally present in the sample matrix, we expect to preserve a similar gain in sensitivity compared to gold-based conventional tests. Furthermore, the long lifetime of Eu<sup>3+</sup> excited states enables the implementation of a cheap time-gated detection system, in case it proves necessary to eliminate non-specific signals due to the matrix. Altogether these results pave the way for a fast, quantitative detection either in low-tech environments or in emergency situations before the patient reaches the hospital.

## **ASSOCIATED CONTENT**

### **Supporting Information**

S1 – Chemicals, salts, and toxins. S2 – Nanoparticle synthesis, functionalization and characterization. S3 – Strip preparation. S4 – Schematic representation of the LEDs arrangement inside the homemade reader. S5 – LFA quantitative analysis of strips labeled with Eu NPs. S6 – LFA sensitivity by visual inspection

of strips labeled with Au and Eu nanoparticles. S7 - Influence of the strip batch on LFA sensitivity. S8 – Non-specific adsorption of nanoparticles on the nitrocellulose membrane. S9 – Non- linear fit of the calibration curves. S10 – Quantitative analysis of strips labeled with gold nanoparticles. S11 – Study of the potential cross-talk in view of multiplexing. S12 – Quantitative analysis of multiplexed strips labeled with Eu nanoparticles. S13 – Multiplexed strips with different toxin concentrations.

## **AUTHOR INFORMATION**

### **Corresponding Author**

\* fanny.mousseau@polytechnique.edu

### **Author Contributions**

The manuscript was written through contributions of all authors. All authors have given approval to the final version of the manuscript. ‡These authors contributed equally.

## **CONFLICTS OF INTEREST**

Antigoni Alexandrou, Cedric Bouzigues, and Thierry Gacoin are co-founders and shareholders of LumediX (Palaiseau, France).

## **ACKNOWLEDGMENTS**

We are grateful to Pascal Preira (Ecole Polytechnique, Laboratory LOB, France) and Max Richly (LumediX, France) for the initial implementation of this approach<sup>47</sup> and to Hervé Boutal, Eric Chabrol, Gérald Theillet, and Thibaut Mercey (LumediX, France) for helpful discussions. We thank Rabei Mohammedi (Ecole Polytechnique, Laboratory PMC, France) for the Eu-doped nanoparticle synthesis, Jean-Marc Sintès and Xavier Solinas (Ecole Polytechnique, Laboratory LOB, France) for their contribution to the reader development, and the LumediX company (Paris, France) for providing access to the facility for strip preparation. This project was funded through the Agence Innovation Défense (AID) grant

SPIDERMAP and the SATT Paris-Saclay project NLISA. For the TEM experiments, the present work has benefited from the Imagerie-Gif core facility supported by l'Agence Nationale de la Recherche (ANR-11-EQPX-0029 / Morphoscope, ANR-10-INBS-04 / FranceBioImaging; ANR-11-IDEX-0003-02 / Saclay Plant Sciences).

## BIBLIOGRAPHY

1. Kosack, C. S., Page, A.-L. & Klatser, P. R. A guide to aid the selection of diagnostic tests. *Bulletin of the World Health Organization* **95**, 639–645 (2017).
2. Gong, X. *et al.* A review of fluorescent signal-based lateral flow immunochromatographic strips. *J. Mater. Chem. B* **5**, 5079–5091 (2017).
3. Bishop, J. D., Hsieh, H. V., Gasperino, D. J. & Weigl, B. H. Sensitivity enhancement in lateral flow assays: a systems perspective. *Lab Chip* **19**, 2486–2499 (2019).
4. Huang, X., Aguilar, Z. P., Xu, H., Lai, W. & Xiong, Y. Membrane-based lateral flow immunochromatographic strip with nanoparticles as reporters for detection: A review. *Biosensors and Bioelectronics* **75**, 166–180 (2016).
5. Mayer, K. M. & Hafner, J. H. Localized Surface Plasmon Resonance Sensors. *Chem. Rev.* **111**, 3828–3857 (2011).
6. Xu, H. *et al.* Gold-Nanoparticle-Decorated Silica Nanorods for Sensitive Visual Detection of Proteins. *Anal. Chem.* **86**, 7351–7359 (2014).
7. Scherr, T. F., Gupta, S., Wright, D. W. & Haselton, F. R. Mobile phone imaging and cloud-based analysis for standardized malaria detection and reporting. *Sci Rep* **6**, 28645 (2016).
8. Bouzigues, C., Gacoin, T. & Alexandrou, A. Biological applications of rare-earth based nanoparticles. *ACS nano* **5**, 8488–8505 (2011).
9. Liao, T. Lanthanide chelate-encapsulated polystyrene nanoparticles for rapid and quantitative immunochromatographic assay of procalcitonin. *RSC Advances* **6**, 103463–103470 (2016).

10. Preechakasedkit, P. *et al.* Gold nanoparticle core–europium( III ) chelate fluorophore-doped silica shell hybrid nanocomposites for the lateral flow immunoassay of human thyroid stimulating hormone with a dual signal readout. *Analyst* **143**, 564–570 (2018).
11. Huhtinen, P. *et al.* Synthesis, Characterization, and Application of Eu(III), Tb(III), Sm(III), and Dy(III) Lanthanide Chelate Nanoparticle Labels. *Anal. Chem.* **77**, 2643–2648 (2005).
12. Cardoso Dos Santos, M. *et al.* Lanthanide-Complex-Loaded Polymer Nanoparticles for Background-Free Single-Particle and Live-Cell Imaging. *Chem. Mater.* **31**, 4034–4041 (2019).
13. Niedbala, R. S. *et al.* Detection of Analytes by Immunoassay Using Up-Converting Phosphor Technology. *Analytical Biochemistry* **293**, 22–30 (2001).
14. He, H. *et al.* Quantitative Lateral Flow Strip Sensor Using Highly Doped Upconversion Nanoparticles. *Anal. Chem.* **90**, 12356–12360 (2018).
15. Wen, S. *et al.* Advances in highly doped upconversion nanoparticles. *Nat Commun* **9**, 2415 (2018).
16. Paterson, A. S. *et al.* Persistent Luminescence Strontium Aluminate Nanoparticles as Reporters in Lateral Flow Assays. *Anal. Chem.* **86**, 9481–9488 (2014).
17. Paterson, A. S. *et al.* A low-cost smartphone-based platform for highly sensitive point-of-care testing with persistent luminescent phosphors. *Lab Chip* **17**, 1051–1059 (2017).
18. Danthararyana, A. N. *et al.* A multicolor multiplex lateral flow assay for high-sensitivity analyte detection using persistent luminescent nanophosphors. *Anal. Methods* **12**, 272–280 (2020).
19. Zhang, F. *et al.* Lanthanide-labeled immunochromatographic strips for the rapid detection of *Pantoea stewartii* subsp. *stewartii*. *Biosensors and Bioelectronics* **51**, 29–35 (2014).
20. Urusov, Zherdev & Dzantiev. Towards Lateral Flow Quantitative Assays: Detection Approaches. *Biosensors* **9**, 89 (2019).
21. Kanchi, S., Sabela, M. I., Mdluli, P. S., Inamuddin & Bisetty, K. Smartphone based bioanalytical and diagnosis applications: A review. *Biosensors and Bioelectronics* **102**, 136–149 (2018).

22. Nelis, J. L. D., Tsagkaris, A. S., Dillon, M. J., Hajslova, J. & Elliott, C. T. Smartphone-based optical assays in the food safety field. *TrAC Trends in Analytical Chemistry* **129**, 115934 (2020).
23. Ghosh, S. K. & Pal, T. Interparticle Coupling Effect on the Surface Plasmon Resonance of Gold Nanoparticles: From Theory to Applications. *Chem. Rev.* **107**, 4797–4862 (2007).
24. Anfossi, L., Di Nardo, F., Cavalera, S., Giovannoli, C. & Baggiani, C. Multiplex Lateral Flow Immunoassay: An Overview of Strategies towards High-throughput Point-of-Need Testing. *Biosensors* **9**, 2 (2018).
25. Lee, S., Mehta, S. & Erickson, D. Two-Color Lateral Flow Assay for Multiplex Detection of Causative Agents Behind Acute Febrile Illnesses. *Anal. Chem.* **88**, 8359–8363 (2016).
26. Mohd Hanafiah, K. *et al.* Development of Multiplexed Infectious Disease Lateral Flow Assays: Challenges and Opportunities. *Diagnostics* **7**, 51 (2017).
27. Wu, S. *et al.* A Review of the Methods for Detection of Staphylococcus aureus Enterotoxins. *Toxins* **8**, 176 (2016).
28. Fisher, E. L., Otto, M. & Cheung, G. Y. C. Basis of Virulence in Enterotoxin-Mediated Staphylococcal Food Poisoning. *Frontiers in Microbiology* **9**, (2018).
29. Beaupaire, E. *et al.* Functionalized Fluorescent Oxide Nanoparticles: Artificial Toxins for Sodium Channel Targeting and Imaging at the Single-Molecule Level. *Nano Letters* **4**, 2079–2083 (2004).
30. Casanova, D. *et al.* Single europium-doped nanoparticles measure temporal pattern of reactive oxygen species production inside cells. *Nature Nanotech* **4**, 581–585 (2009).
31. Türkcan, S., Richly, M. U., Bouzigues, C. I., Allain, J.-M. & Alexandrou, A. Receptor Displacement in the Cell Membrane by Hydrodynamic Force Amplification through Nanoparticles. *Biophysical Journal* **105**, 116–126 (2013).
32. Abdesselem, M. *et al.* Multifunctional Rare-Earth Vanadate Nanoparticles: Luminescent Labels, Oxidant Sensors, and MRI Contrast Agents. *ACS Nano* **8**, 11126–11137 (2014).

33. Wang, W. *et al.* Gold-Nanoparticle-Based Multiplexed Immunochromatographic Strip for Simultaneous Detection of Staphylococcal Enterotoxin A, B, C, D, and E. *Part. Part. Syst. Charact.* **33**, 388–395 (2016).
34. Féraudet Tarrisse, C. *et al.* Highly sensitive and specific detection of staphylococcal enterotoxins SEA, SEG, SEH and SEI by immunoassay. *Toxins* **13**, 130 (2021).
35. Lefebvre, D. *et al.* Quantitative Determination of *Staphylococcus aureus* Enterotoxins Types A to I and Variants in Dairy Food Products by Multiplex Immuno-LC-MS/MS. *J. Agric. Food Chem.* **69**, 2603–2610 (2021).
36. Huignard, A., Gacoin, T. & Boilot, J.-P. Synthesis and Luminescence Properties of Colloidal YVO<sub>4</sub>:Eu Phosphors. *Chem. Mater.* **12**, 1090–1094 (2000).
37. Huignard, A., Buissette, V., Franville, A.-C., Gacoin, T. & Boilot, J.-P. Emission Processes in YVO<sub>4</sub>:Eu Nanoparticles. *J. Phys. Chem. B* **107**, 6754–6759 (2003).
38. Casanova, D. *et al.* Counting the Number of Proteins Coupled to Single Nanoparticles. *J. Am. Chem. Soc.* **129**, 12592–12593 (2007).
39. Giaume, D. *et al.* Organic Functionalization of Luminescent Oxide Nanoparticles toward Their Application As Biological Probes. *Langmuir* **24**, 11018–11026 (2008).
40. de Puig, H., Bosch, I., Gehrke, L. & Hamad-Schifferli, K. Challenges of the Nano–Bio Interface in Lateral Flow and Dipstick Immunoassays. *Trends in Biotechnology* **35**, 1169–1180 (2017).
41. Jain, N. *et al.* Synthesis and Rational design of Europium and Lithium Doped Sodium Zinc Molybdate with Red Emission for Optical Imaging. *Sci Rep* **9**, 2472 (2019).
42. Riwotzki, K. & Haase, M. Wet-Chemical Synthesis of Doped Colloidal Nanoparticles: YVO<sub>4</sub>:Ln (Ln = Eu, Sm, Dy). *J. Phys. Chem. B* **102**, 10129–10135 (1998).
43. Armbruster, D. A. & Pry, T. Limit of Blank, Limit of Detection and Limit of Quantitation. *Clin Biochem Rev* **29**, 4 (2008).

44. VIDAS® Staph enterotoxin II (SET2) - user instructions; bioMérieux SA, Marcy l'Etoile, France.
45. RIDASCREEN® SET A,B,C,D,E - user instructions; R-Biopharm AG, Darmstadt, Germany.
46. Byzova, N. A., Safenkova, I. V., Slutskaya, E. S., Zherdev, A. V. & Dzantiev, B. B. Less is More: A Comparison of Antibody–Gold Nanoparticle Conjugates of Different Ratios. *Bioconjugate Chem.* **28**, 2737–2746 (2017).
47. Preira, P., Richly, M. U., Bouzigues, C. & Alexandrou, A. Test à diffusion capillaire mettant en œuvre des nanoparticules inorganiques photoluminescentes.

## Supplementary Information

# Luminescent lanthanide nanoparticle-based imaging enables ultra-sensitive, quantitative and multiplexed *in vitro* Lateral Flow Immunoassays

F. Mousseau<sup>a\*</sup>, C. Féraudet Tarrisse<sup>b</sup>, S. Simon<sup>b</sup>, T. Gacoin<sup>c</sup>, A. Alexandrou<sup>a†</sup> and C. I. Bouzigues<sup>a†</sup>

<sup>a</sup>: *Laboratoire d'Optique et Biosciences, Ecole Polytechnique, Institut Polytechnique de Paris, CNRS, INSERM, Route de Saclay, 91128 Palaiseau, France.*

<sup>b</sup>: *Université Paris-Saclay, CEA, INRAE, Département Médicaments et Technologies pour la Santé (DMTS), 91191 Gif-sur-Yvette, France.*

<sup>c</sup>: *Laboratoire de Physique de la Matière Condensée, Ecole Polytechnique, Institut Polytechnique de Paris, CNRS, Route de Saclay, 91128 Palaiseau, France.*

### Outline

---

|   |    |
|---|----|
| S1 – Chemicals, salts and toxins .....  | 2  |
| S2 – Nanoparticle synthesis, functionalization and characterization .....                     | 3  |
| S3 – Strip preparation.....   | 7  |
| S4 – Schematic representation of the LEDs arrangement inside the homemade reader.....         | 8  |
| S5 – LFA quantitative analysis of strips labeled with Eu NPs .....                            | 9  |
| S6 – LFA sensitivity by visual inspection of strips labeled with Au and Eu nanoparticles..... | 10 |
| S7 - Influence of the strip batch on LFA sensitivity .....                                    | 11 |
| S8 – Non-specific adsorption of nanoparticles on the nitrocellulose membrane.....             | 12 |
| S9 – Non-linear fit of the calibration curves.....  | 13 |
| S10 - Quantitative analysis of strips labeled with gold nanoparticles .....                   | 14 |
| S11 - Study of the potential cross-talk in view of multiplexing.....                          | 15 |
| S12 – Quantitative analysis of multiplexed strips labeled with Eu nanoparticles.....          | 16 |
| S13 – Multiplexed strips with different toxin concentrations.....                             | 17 |
| References.....   | 18 |

---

Corresponding author: [fanny.mousseau@polytechnique.edu](mailto:fanny.mousseau@polytechnique.edu)

## S1 – Chemicals, salts and toxins

### S1.1 Chemical and salts

Europium (III) nitrate pentahydrate, sodium orthovanadate, succinic anhydride, N-(3-dimethylaminopropyl)-N'-ethylcarbodiimide hydrochloride (EDC), N-hydroxysulfosuccinimide sodium salt (NHS), ethanolamine hydrochloride, sodium azide, glycerol, potassium dihydrogen phosphate ( $\text{KH}_2\text{PO}_4$ ), dipotassium hydrogen phosphate ( $\text{K}_2\text{HPO}_4$ ), sodium dihydrogen phosphate ( $\text{NaH}_2\text{PO}_4$ ), disodium hydrogen phosphate ( $\text{Na}_2\text{HPO}_4$ ), sodium chloride (NaCl), Trizma<sup>®</sup> hydrochloride (Tris-HCl), bovine serum albumin (BSA), MES sodium salt, phosphate buffer saline (PBS) and N-N-dimethylformamide (DMF) were purchased from Sigma Aldrich.

Sodium hydroxide ( $\text{NaOH}$ ,  $10 \text{ mol.L}^{-1}$ ), (3-aminopropyl)triethoxysilane (APTES) and D-glucose came from Fisher Chemicals.

Yttrium (III) nitrate hexahydrate, Tween 20 and absolute ethanol were provided by Merck.

Glycine and ethanol (96 v%) were supplied by VWR Chemicals (Prolabo, GPR recapter).

Rhodamine 6G, the protein assay dye reagent concentrate (Bradford) and the Pierce BCA protein assay kit were purchased respectively from ACROS Organics, Biorad and Thermo Scientific.

### S1.2 Toxin production

Briefly, the DNA sequences of the *sea*, *seg*, *seh* and *sei* genes were obtained from the publicly available genetic sequence database GenBank and optimized for protein expression in the bacterium *E. Coli*. The optimized DNA sequences were inserted in plasmids, enabling their internalization by the bacteria and the production of the corresponding toxins. After culture of *E. Coli* bacteria to induce their proliferation, toxins were extracted and purified by chromatography. More details are available in our previous work<sup>1</sup>.

## S2 – Nanoparticle synthesis, functionalization and characterization

### 1) Synthesis and functionalization of europium-doped nanoparticles

YVO<sub>4</sub>:Eu nanoparticles of YVO<sub>4</sub> doped with 40 % of europium were synthesized by aqueous co-precipitation following a protocol adapted from our previous work<sup>2</sup>. Briefly, two aqueous solutions of 25 ml of the precursor salts were freshly prepared. One contained 0.1 M of sodium orthovanadate and the other contained yttrium nitrate at 0.06 M and europium nitrate at 0.04 M in Milli-Q water. The solution of lanthanides was then rapidly added into the solution of vanadate under vigorous stirring. After 5 min, the pH of the solution was adjusted to pH 9 through the addition of 1 N NaOH. After 2 hours of ageing, the solution was centrifuged at 2 630 g for 20 min. The precipitate was then redispersed in pure water and sonicated for 2 min with a 450 W Branson sonifier. These centrifugation/redispersion steps were repeated 3 times to ensure the removal of counter-ions, as attested by a conductivity lower than 100  $\mu\text{S}\cdot\text{cm}^{-1}$ . The final solution, with a volume adjusted to 50 ml, was then centrifuged at 789 g for 5 min to remove possible aggregates. The resulting colloidal suspensions of YVO<sub>4</sub>:Eu (40 %) NPs was homogeneous and slightly light diffusing.

Particles were then silicated, aminated and carboxylated according to previous work<sup>3,4</sup> to enable their covalent coupling with antibodies (Figure S2.1). In short, 2.5 mL of sodium silicate were added dropwise to 25 mL of nanoparticles at 20 mM of vanadate. The suspension was stirred over night at room temperature and purified as detailed above. Then, 75 mL of silicated NPs at 3 mM of vanadate were added at 1 mL $\cdot\text{min}^{-1}$  using a peristaltic pump to 225 mL of boiling ethanol containing 265  $\mu\text{L}$  of APTES. The reaction solution was further refluxed for 24 hours to ensure the formation of a uniform cross-linked aminated network around the NPs, leading to a covalent shell of amines surrounding the particles. The NPs were purified as described previously but with particle redispersion in an ethanol:water mixture (3:1) instead of pure water. Finally, particles were transferred into DMF and 1 mL of these NPs at 40 mM of vanadate were added to 10 mL of succinic anhydride (0.1 g $\cdot\text{mL}^{-1}$  in DMF). The suspension was stirred overnight under inert atmosphere and purified by 3 cycles of centrifugation/dispersion in MES buffer (50 mM, pH 5 to 6).

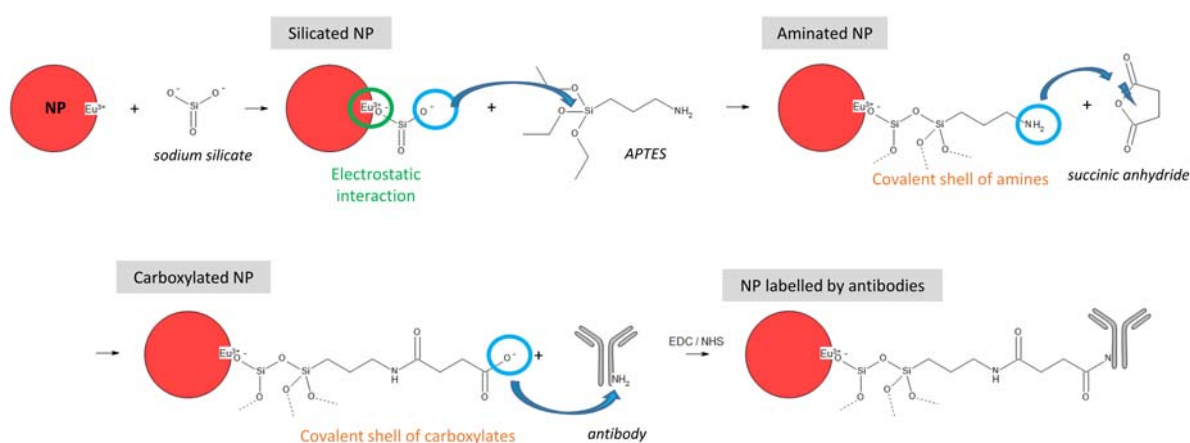


Figure S2.1: Europium-doped nanoparticle functionalization and coupling to detection antibodies.

## 2) Nanoparticle characterization

### Au NPs

Gold NPs (BBI Solutions, EM.GC40, Batch 200 600 92, geometric diameter: 40.8 nm – standard deviation: 8 %) were characterized as received by several techniques. Their hydrodynamic diameter was determined with the Zetasizer Nano ZS equipment (Malvern Instruments, UK). Measurements were performed in triplicate at 25 °C after an equilibration time of 120 s. Nanoparticles exhibited a diameter of 41.4 nm, in agreement with the size determined via transmission electron microscopy by the supplier.

The absorbance of the Au NPs was measured on a UV-1700 pharmaSpec spectrophotometer (Shimadzu), as displayed in Figure S2.2. The surface plasmon resonance peak was observed at 526 nm, which is in agreement with the particle diameter<sup>5</sup>. The Au NPs molar extinction coefficient at 450 nm,  $\epsilon_{450}$ , was estimated to be  $\epsilon_{450} = 5.32 \times 10^9 \text{ cm}^{-1} \cdot \text{L} \cdot \text{mol}^{-1}$  from their size<sup>5</sup>. Using the absorbance of the NPs at 450 nm, we determined the Au NP molar concentration to be equal to  $0.357 \text{ nmol} \cdot \text{L}^{-1}$ . Assuming 59 atoms per  $\text{nm}^3$  of gold nanoparticle, this molar concentration was converted to mass concentration<sup>6</sup>, giving a stock solution at  $150 \mu\text{g} \cdot \text{mL}^{-1}$ .

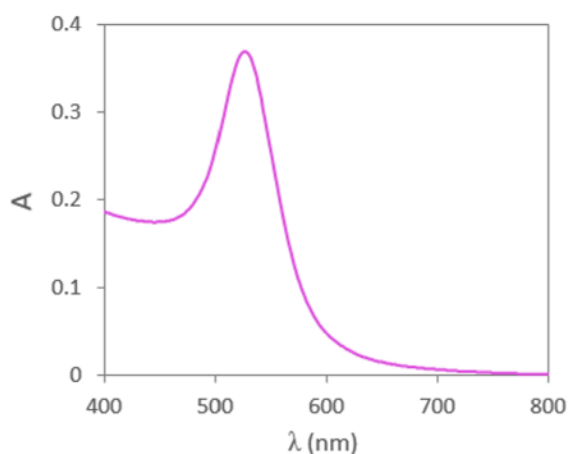


Figure S2.2: Absorbance spectrum of the gold nanoparticles in the visible range (dilution of the stock solution: 1/11 in Milli-Q water).

### Eu NPs

The europium-doped NPs were characterized after synthesis and after each functionalization step. Basically, the size distributions, charge and the spectral properties were obtained by dynamic light scattering (DLS) and transmission electron microscopy (TEM), zeta potential measurements, and UV-vis spectroscopy, respectively.

For the TEM measurements, 2  $\mu\text{L}$  of NP solution was deposited on a formvar/carbon-coated 400 mesh copper grid for 3 min. Then the solution in excess was absorbed by a filter paper and the grid was air dried. NPs were observed on a JEOL JEM-1400 microscope operating at 120 kV. Images were acquired with a high-speed camera (SC1000 Orius, Gatan), processed with Digital Micrograph (Gatan) and analysed quantitatively with the ImageJ software. The inset of the Figure S2.3a displays a TEM image of the Eu NPs. It shows that they are oblong and that their contours are not well defined. This is because Eu NPs are a polycrystalline assembly of monocrystalline grains with a low degree of crystallinity<sup>7</sup>. In addition, following the drying inherent in the preparation of the samples, the nanoparticles are aggregated, which makes it difficult to visualize isolated particles. Nevertheless, short and long axis were manually measured for more than 200 nanoparticles giving mean values of  $26.3 \pm 13.5 \text{ nm}$  and  $12.0 \pm 5.6 \text{ nm}$ , the size distribution being displayed in Figure S2.3a and Figure S2.3b, respectively. Knowing that the crystalline cell of the vanadate matrix ( $7.123 \text{ \AA} \times 7.123 \text{ \AA} \times 6.291 \text{ \AA}$ ) contains four

$Y_{0.6}VO_4Eu_{0.4}$  units, the parameters determined by TEM lead us to estimate that 1 mM of vanadate corresponds to 22.9 nM of NPs<sup>8</sup>.

The hydrodynamic diameter of the nanoparticles, based on the intensity distribution obtained from the dynamics light scattering measurements, were, respectively, 180, 130, 160 and 130 nm for the bare, silicated, aminated and carboxylated nanoparticles. This large diameters are probably due to the relative polydispersity of the nanoparticles and to the fact that DLS measurements, in particular the intensity distribution, strongly overestimate the contribution of larger particle sizes.

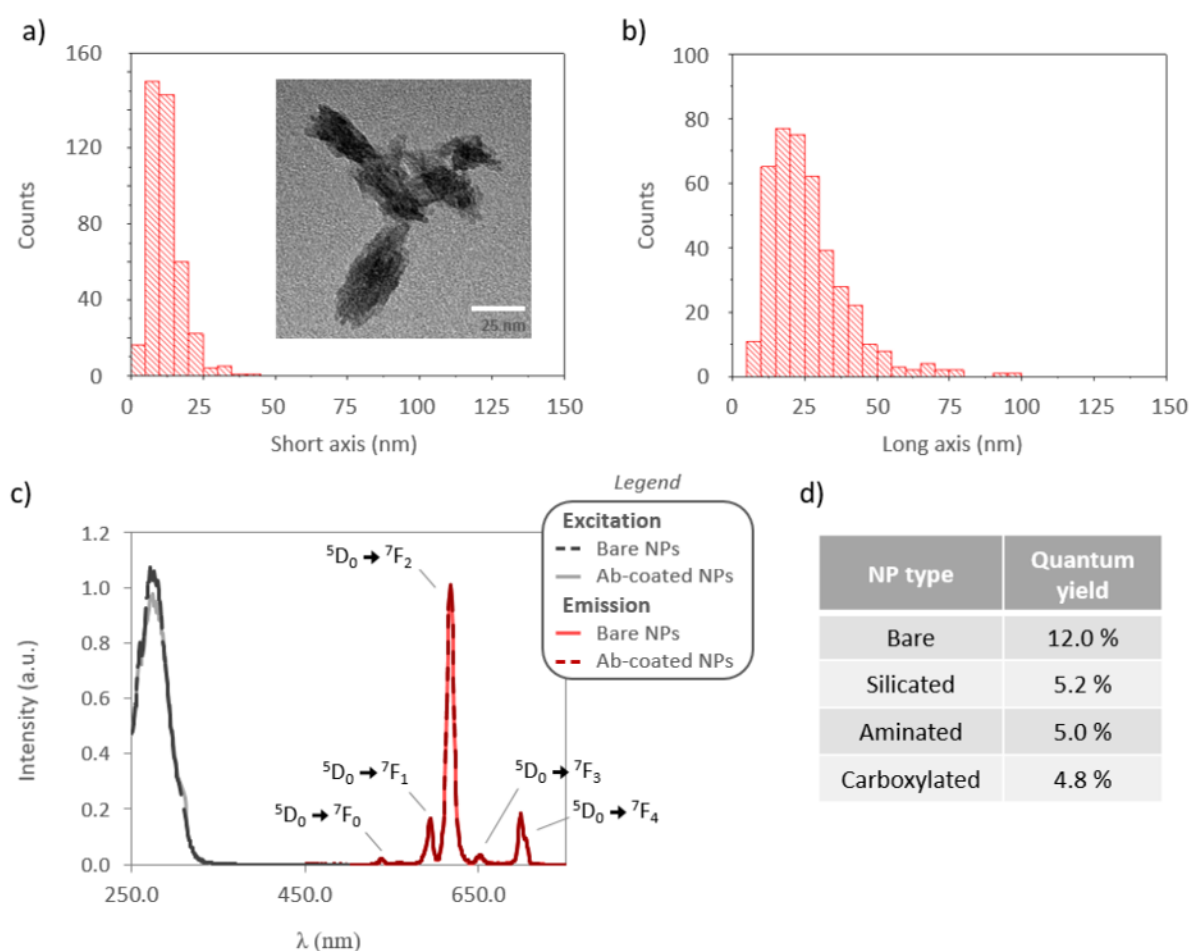


Figure S2.3: a, b) Size distribution of the short (a) and long (b) axis of the Eu NPs from TEM images. Inset: example of a TEM image. c) Excitation (grey lines) and emission (red lines) spectra of the europium-doped nanoparticles either bare (dashed lines) or coupled to antibodies (continuous lines). Nanoparticles were diluted in Milli-Q water at 10  $\mu$ M of vanadate ions. The excitation spectrum was obtained for the emission wavelength of 617 nm while the emission spectrum was obtained by exciting the particles at 280 nm. The signal intensity  $I$  was expressed in arbitrary units (a.u.). d) Quantum yield of bare, silicated, aminated and carboxylated nanoparticles. After an initial decrease of the quantum yield upon silica coating, the subsequent functionalization steps did not modify the nanoparticle quantum yield.

The zeta potential was determined with the Zetasizer Nano ZS equipment (Malvern Instruments, UK) for particles at 0.4 mM of vanadate ions. Measurements were performed in triplicate at 25 °C after an equilibration time of 120 s. Bare, silicated, aminated and carboxylated nanoparticles exhibited a zeta potential at +27, -16, +28 and -14, suggesting that the successive functionalization steps ran smoothly. Excitation and emission spectra were recorded on Cary Eclipse Varian fluorometer for nanoparticles at 10  $\mu$ M of vanadate ions in Milli-Q water, showing that Eu NPs exhibit maximum absorbance and luminescence at 280 nm and 617 nm, respectively (Figure S2.3c).

The quantum yield was determined by the “Relative Determination Method”<sup>9</sup>. Absorption (Shimadzu spectrophotometer) and fluorescence spectra (Fluorolog®, Horiba) were measured for Rhodamine 6G (5 μM) and Eu-doped nanoparticles (10 μM of vanadate) in absolute ethanol and pure water, respectively. The quantum yield  $\Phi$  was then calculated following the formula of Demas and Crosby:

$$\Phi = \Phi_r \cdot \left(\frac{n_s}{n_r}\right)^2 \cdot \frac{1 - 10^{-A_r}}{1 - 10^{-A_s}} \cdot \frac{I_s}{I_r} \cdot \frac{f_r}{f_s}$$

In this equation, the subscripts s and r denote the sample and the reference,  $\Phi_r$  is the fluorescence quantum yield of the reference (here 0.95),  $n$  is the refractive index of the solvents ( $n_s = 1.33$  for water and  $n_r = 1.36$  for absolute ethanol),  $A$  denotes the absorbance at the excitation wavelength employed for the fluorescence spectra measurement (here 280 nm),  $I$  represents the spectrally integrated fluorescence signal and  $f$  is the instrumental function. Fixing the same measurement parameters (excitation wavelength, slit width, integration times, spectral range, ...) for the sample and the reference ensured  $f_s = f_r$ . With this protocol, the quantum yield of the nanoparticles was determined for the different surface functionalization (Figure S2.3.d). Results show that bare NPs have a quantum yield of 12 %. Silica coating induces a significant decrease in the quantum yield, which however remains constant at around 5 % after the next surface modification steps.

### 3) Nanoparticle coupling to antibodies

Detection antibodies were adsorbed on gold nanoparticles according to the following protocol. Briefly, 100 μL of antibodies (250 μg.mL<sup>-1</sup> in potassium phosphate buffer – 2 mM, pH 7.4) were added to 800 μL of nanoparticles (350 pM) and the solution was stirred in the dark for 1 h. Then, 100 μL of a precipitating solution (1 % of BSA in potassium phosphate buffer – 20 mM, pH 7.4) was added to the suspension prior to purification by 2 cycles of centrifugation (15 min, 15 000 g) and dispersion in a conservation solution (0.1 % of BSA in potassium phosphate buffer - 2 mM, pH 7.4).

Detection antibodies were covalently bound to the Eu-doped nanoparticles. To this aim, the carboxylic functions of the NPs (1 μmol of vanadate ions) were activated by 430 μL of an EDC / NHS mixture (0.5 mg.mL<sup>-1</sup> of each reactant in MES buffer) during 25 min under stirring. The excess of EDC / NHS was removed by centrifugation and NPs were re-suspended in 125 μL of antibody solution (final concentration: 0.55 mg.mL<sup>-1</sup> in MES), giving an Ab to NP molar ratio of 20. After 1 h of incubation at 37 °C under stirring, the particles were transferred to a blocking buffer (2 % of BSA and 100 mM of ethanolamine hydrochloride in PBS) for 1 h of passivation, then purified by alternating centrifugation and dispersion in a conservation buffer (0.05 % of Tween20, 0.1 % of glycine and 10 % of glycerol in potassium phosphate buffer – 10 mM, pH 7.4). Note that the coupling ratio was verified before the passivation step with a Bradford assay performed on the supernatant and a BCA assay carried out on the nanoparticle pellet. A coupling efficiency close to 100% was obtained.

Excitation and emission spectra of the coupled nanoparticles were recorded as described above and displayed in Figure S2.3.c. The spectra of bare and antibody-conjugated nanoparticles are superimposable. Considering in addition that the quantum yield of the nanoparticles seems affected only by the first step of their surface modification (as discussed previously), we may assume that the excitation and emission spectra of the coupled NPs as well as their quantum yield will not be modified in more complex environments like in sample matrices or in LFA strips.

## S3 – Strip preparation

### S3.1 – Treatment, assembly, cutting and conservation of strips

After antibody deposition on the nitrocellulose, membranes were treated to limit non-specific signals, surface corrosion or antibody denaturation induced by the complex interactions arising between the inorganic reporters, the nitrocellulose and the antibodies<sup>10</sup>. Briefly, membranes were dried at 37 °C for 20 min, immersed 30 min in a saturation solution (0.5 % BSA and 150 mM NaCl in sodium phosphate buffer - 10 mM, pH 7.4), rinsed with Milli-Q water, incubated 20 min in a conservation solution (0.1 % Tween 20 and 7.5 % glucose in sodium phosphate buffer - 10 mM, pH 7.4) and dried at 37 °C for 20 min. Subsequently, an absorption pad (SureWick CFSP 203000, Merck) and a conjugate pad (Glass Fiber Diagnostic Pad GFDX 083000, Merck) were attached, overlapping the nitrocellulose membrane on 2 mm. This assembled membrane card was hand-rolled to ensure adhesion of the different components and was then cut into 5 mm wide strips using a CM5000™ Guillotine Cutter (BioDot, USA). The prepared strips were then stored with desiccant at room temperature before use.

### S3.2 - Influence of the test line position on LFA sensitivity for multiplex strip preparation

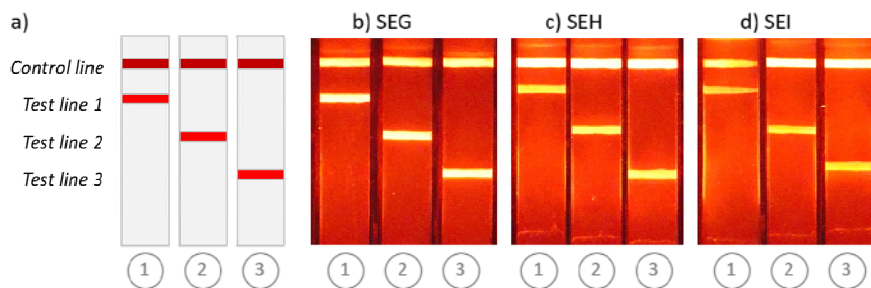


Figure S3.1: a) Representation of the strips designed to study the influence of the test line position on the assay sensitivity. b-d) Assays performed with the toxins SEG (b), SEH (c), and SEI (d) at 1 ng.mL<sup>-1</sup> using Eu NP probes.

### S3.3 – Performing an LFA assay in a dipstick format

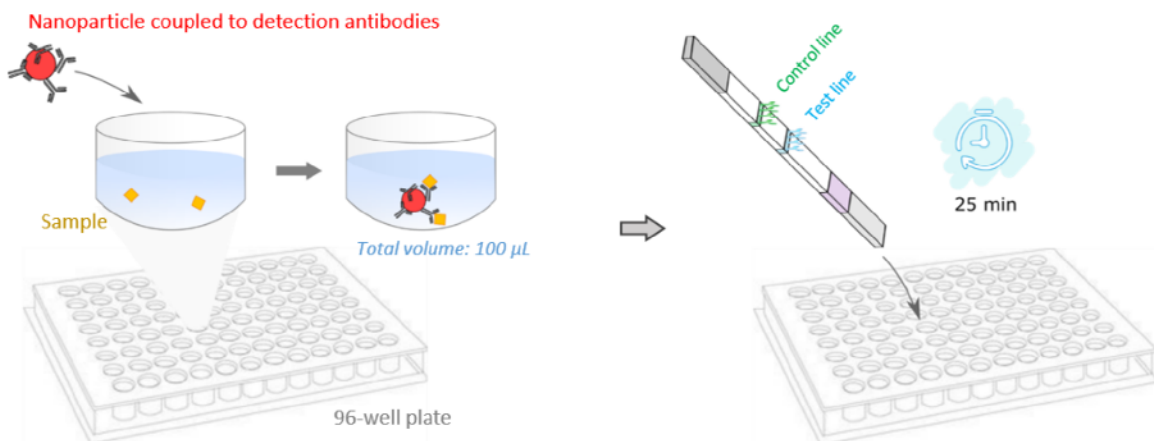


Figure S3.2: Schematic representation of how we perform LFA assays in the dipstick format.

S4 – Schematic representation of the LEDs arrangement inside the homemade reader

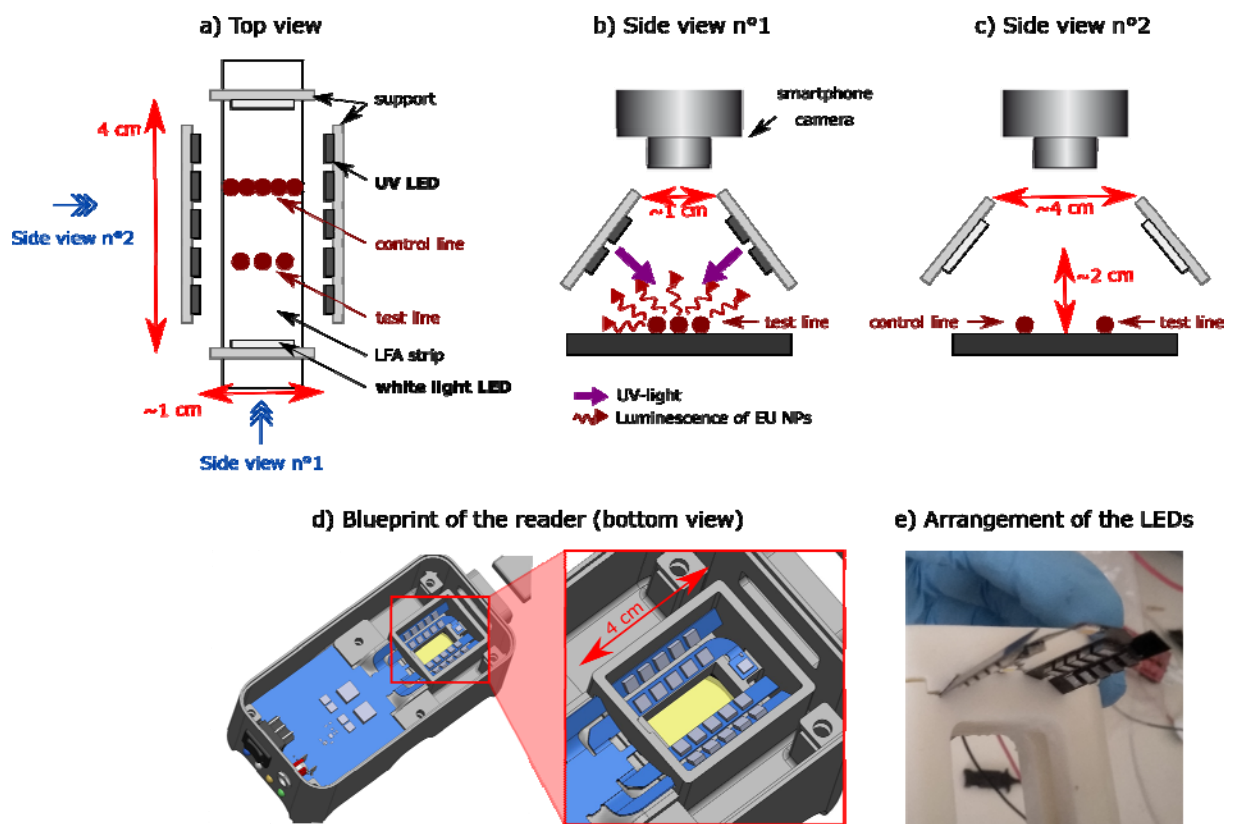


Figure S4: a) Top view of the arrangement of UV LEDs and white light LEDs above the LFA strip. The camera has been removed from this scheme for clarity. b) Side view n°1. The white light LEDs, which are in the foreground and in the background, have not been shown to simplify the visualization of the assembly. c) Side view n°2. The UV LEDs, which are foreground and background in this view, are not displayed to help to visualize the system. d) Blueprint displaying a bottom view of the reader (BitMaker, Paris). The inset shows the 20 UV LEDs (2 mW LEUVK37B50HF00, Laser Components) and the 2 white light LEDs. e) Picture of the arrangement of the LEDs leading to a typical excitation intensity of  $\sim 4 \text{ mW/cm}^2$ .

## S5 – LFA quantitative analysis of strips labeled with Eu NPs

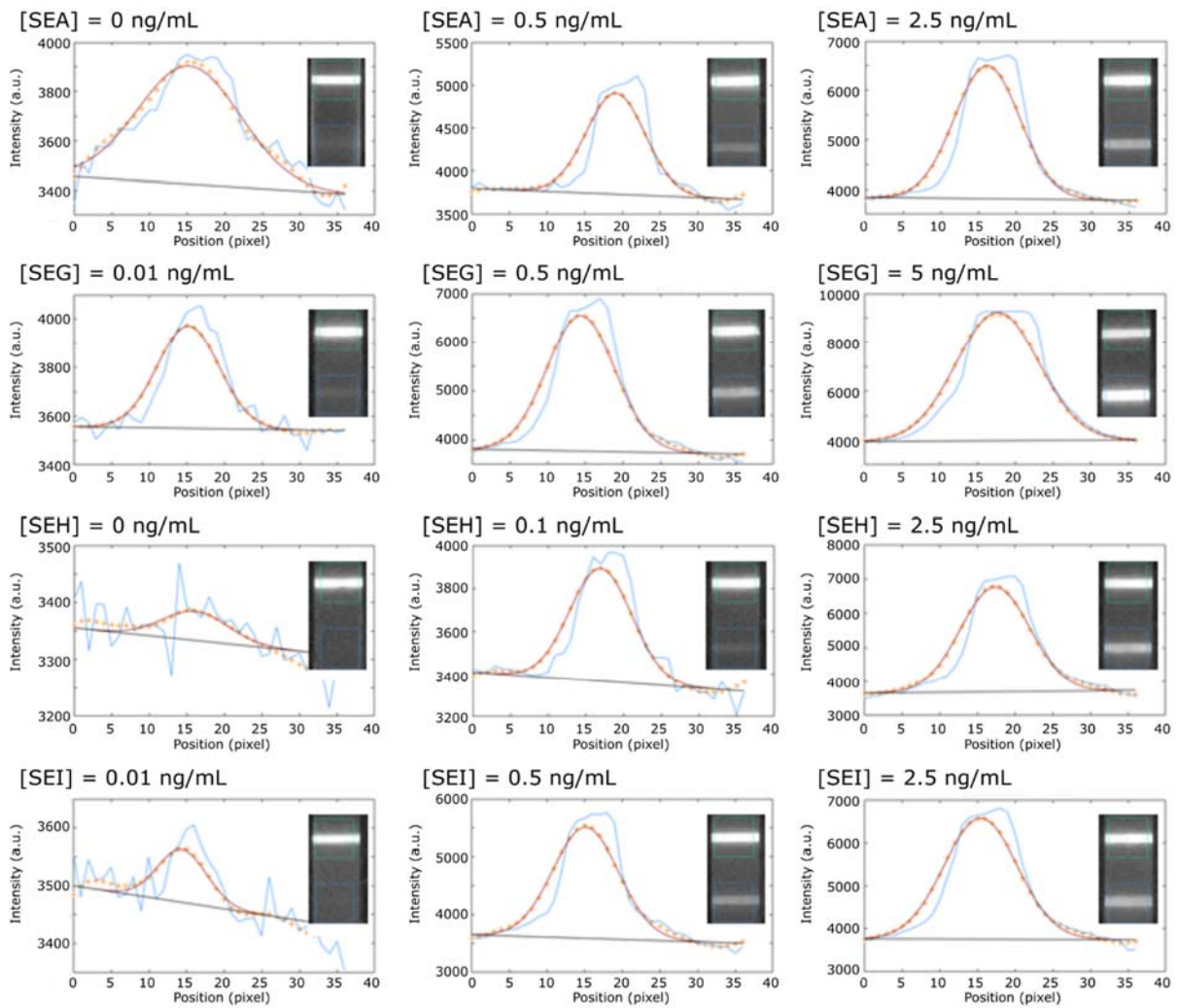


Figure S5: Examples of LFA quantitative analysis for strips labeled with Eu NPs. The raw data are in blue, the curves after convolution by a Gaussian function are in orange. The Gaussian fits of the convoluted data and the background are respectively in red and grey. Note that the ordinate scale varies from one graph to another, thus making it possible to show that the data analysis is suitable regardless of the amplitude of the peak and the associated noise. Insets show strips with green and blue rectangles indicating the ROI localization around the control and test lines, respectively.

S6 – LFA sensitivity by visual inspection of strips labeled with Au and Eu nanoparticles

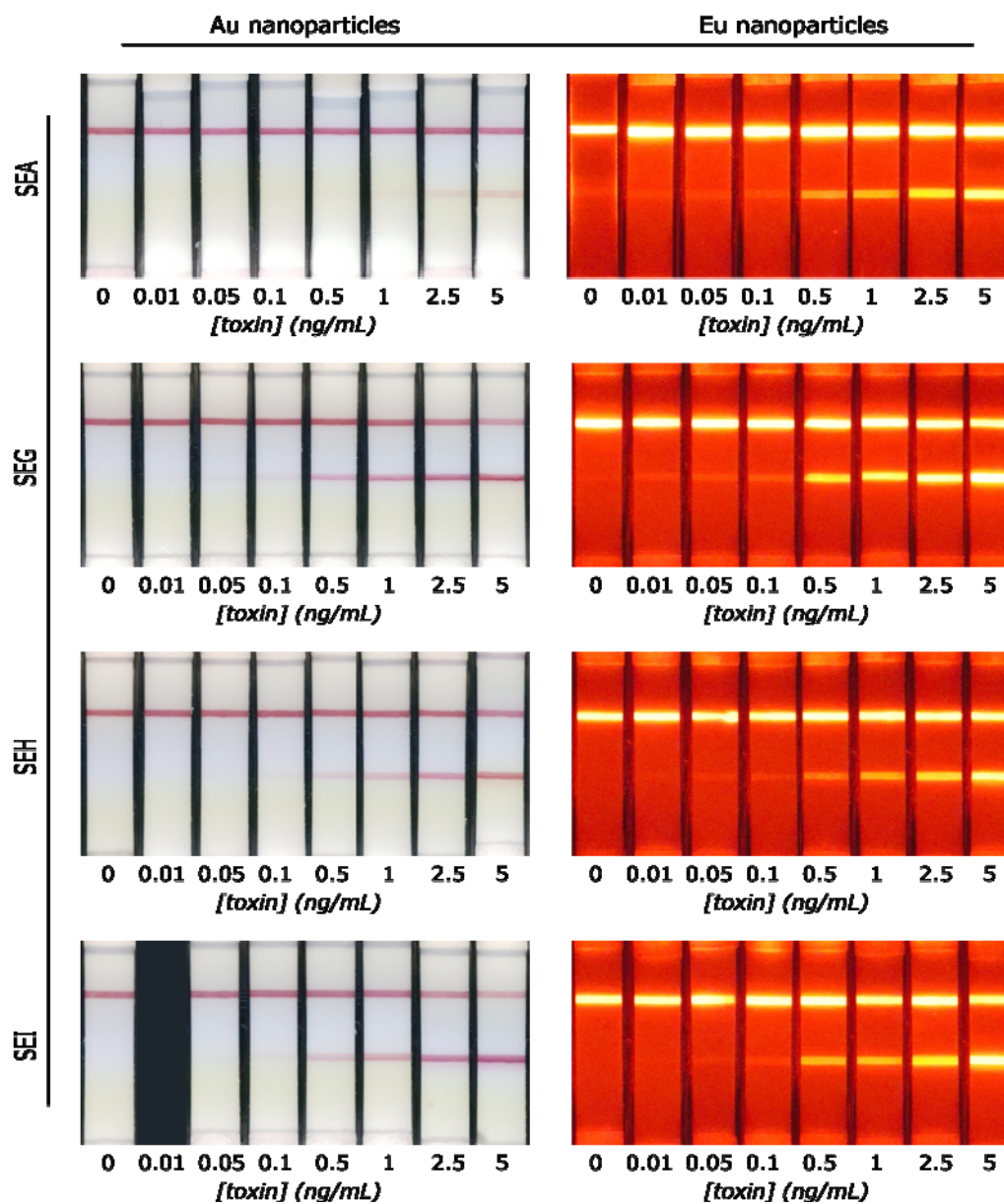


Figure S6: LFA strips labeled with gold and europium-doped nanoparticles for the detection of the SEA, SEG, SEH, and SEI toxins (concentrations ranging from 0.01 to 5 ng.mL<sup>-1</sup>).

| NPs         | Sensitivity (ng.mL <sup>-1</sup> ) |           |           |           |
|-------------|------------------------------------|-----------|-----------|-----------|
|             | SEA                                | SEG       | SEH       | SEI       |
| Au          | 2.5                                | 0.1       | 0.5       | 0.5       |
| Eu          | 0.5                                | 0.01      | 0.05      | 0.05      |
| <b>Gain</b> | <b>5</b>                           | <b>10</b> | <b>10</b> | <b>10</b> |

Table S6: Approximate lowest detectable concentrations and sensitivity gains obtained by visual inspection of the strips labeled with Au and Eu NPs.

S7 - Influence of the strip batch on LFA sensitivity

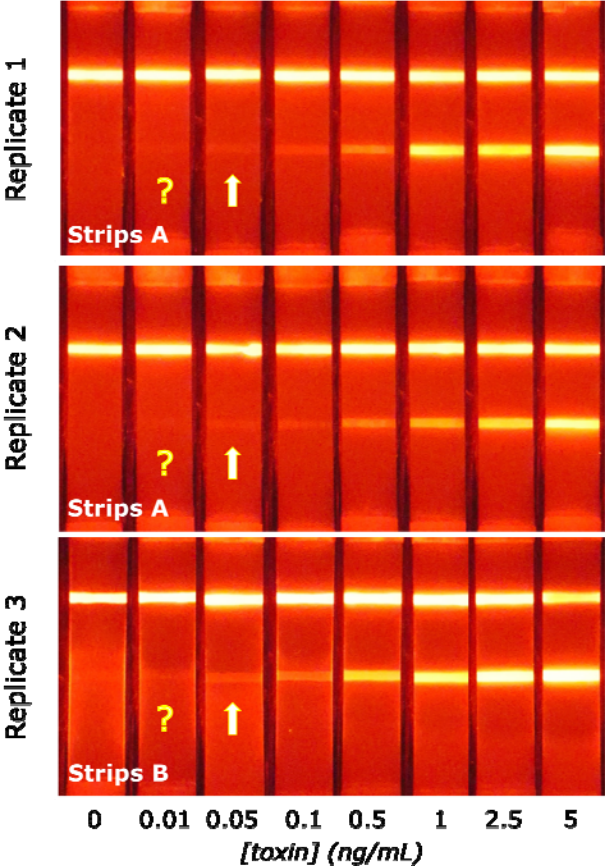


Figure S7: LFA strips labeled with europium-doped nanoparticles for the detection of SEH (from 0.01 to 5 ng.mL<sup>-1</sup>). The first two replicates are made with a first batch of strips (strips A), the third one with a second batch (strips B) made from the same batches of nitrocellulose membrane, sample pad, absorption pad and antibodies. The difference between the two strip batches is the day of the strip preparation.

## S8 – Non-specific adsorption of nanoparticles on the nitrocellulose membrane

LFA were performed in the absence or presence of europium-doped nanoparticles. The mean value of the intensity of the R, G, and B channels of the pictures were measured on the strip – including autofluorescence and non-specifically adsorbed nanoparticles - and on the strip holder in the Regions Of Interest (ROIs) shown in Figure S8. The final signal, defined as the difference between intensities coming from the strip and the holder, was typically 2 times higher in the presence of the Eu NPs. These results indicated that a significant part of the background was not due to the autofluorescence of the strip but rather to the non-specific adsorption of nanoparticles all along the strip during migration. This showed that, in our acquisition regime, autofluorescence did not prevent from reliably detecting the lowest nanoparticle concentrations deposited on the strip. This phenomenon was not limited to our luminescent particles: by imaging fully dried strips (1 days) labelled with gold NPs, non-specific adsorption was also observed (data not shown).

The sensitivity was thus not limited by the minimal number of detectable probes but by the residual signal coming from the non-specific adsorption of NP-Ab conjugates along the strip.

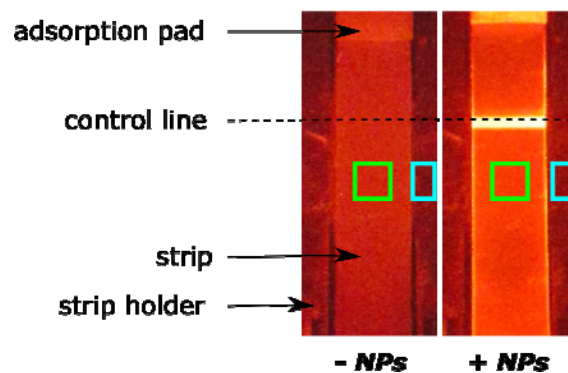


Figure S8: Typical LFA performed without toxin in the presence or absence of Eu NPs for the same nanoparticle concentration as the one used in the toxin experiments. Intensities were measured via ImageJ in the green and blue Regions Of Interest (ROIs) respectively placed on the strip and strip holder. The values were respectively 87 and 59 for the strip and its holder in the absence of NPs, and 104 and 59 in the presence of the latter, giving final signals of respectively 28 and 45 in the absence and presence of particles.

S9 – Non-linear fit of the calibration curves

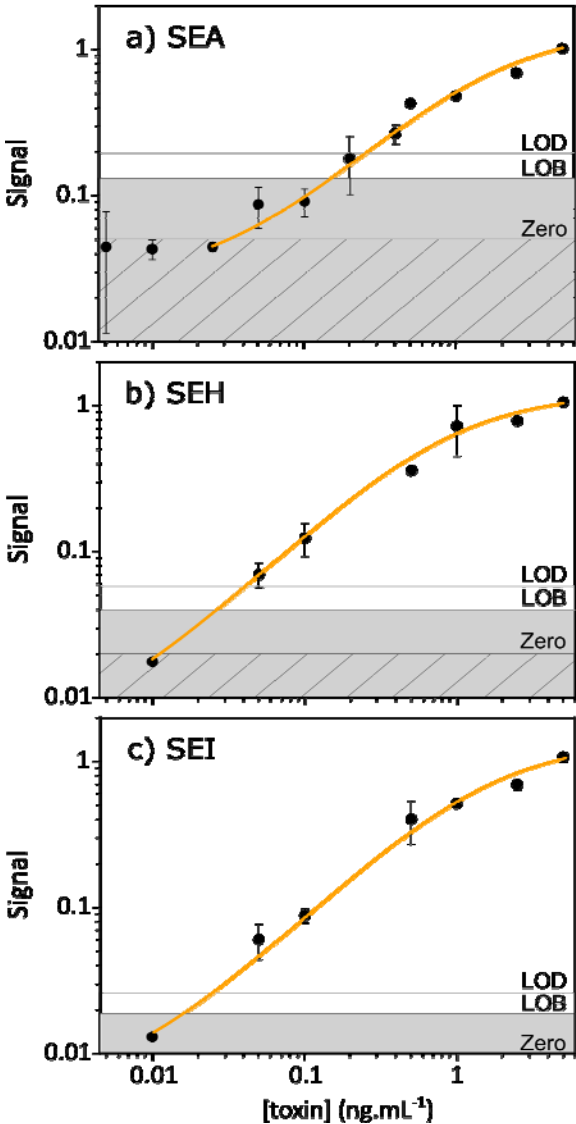


Figure S9: Quantitative analysis of range of SEA (a), SEH (b), and SEI (c) concentrations obtained in independent duplicates with Eu-doped NPs as probes (error bars indicate the standard deviation of two independent replicates). The experimental data are fitted (orange curves) by  $Signal = A.[toxin] / (B + [toxin]) + C$ . The obtained constants A, B, C, and the fit residuals respectively equal 1.29, 1.79, 0.02, and 0.98 for SEA, 1.18, 0.89, 0.005, and 0.99 for SEH, and 1.32, 1.58, 0.005, and 0.99 for SEI.

S10 - Quantitative analysis of strips labeled with gold nanoparticles

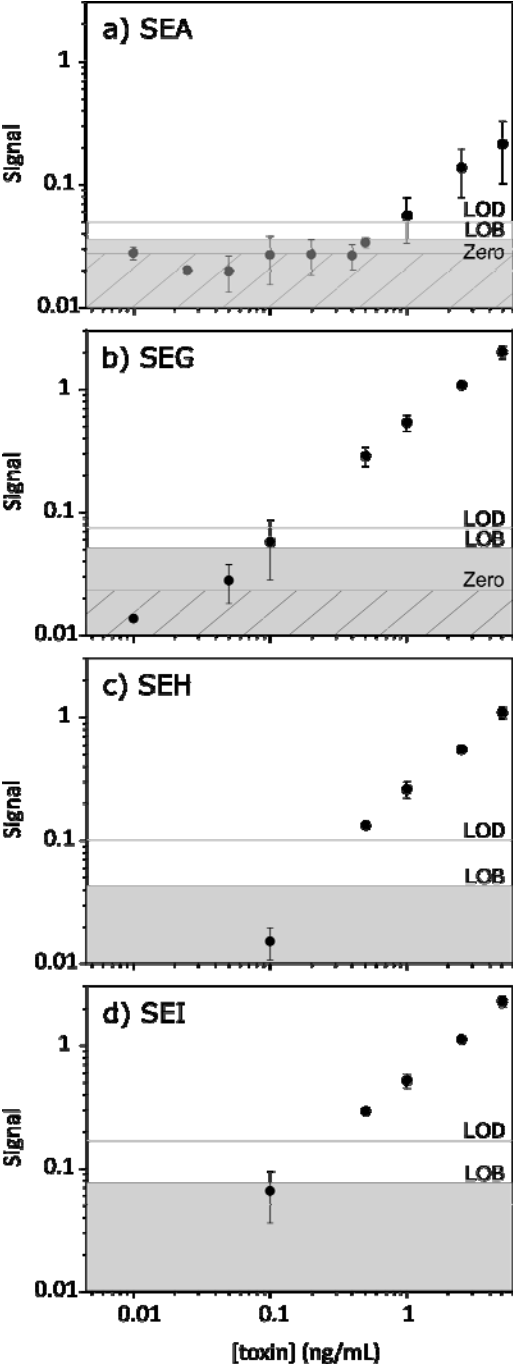


Figure S10: Quantitative analysis of range of SEA (a), SEG (b), SEH (c), and SEI (d) concentrations obtained in independent duplicates with gold NPs as probes (error bars indicate the standard deviation of two independent replicates). The zero, LOB and LOD are calculated from 8 independent replicates performed in the absence of toxin (zero =  $mean_0$ , LOB =  $mean_0 + 1.645 SD_0$  and LOD =  $mean_0 + 3 SD_0$ , where the mean value of the test line signal in the absence of toxin is abbreviated  $mean_0$  and its standard deviation  $SD_0$ ).

## S11 - Study of the potential cross-talk in view of multiplexing

All the “test line / toxin / Eu NPs” combinations are tested in simplex LFA labeled by Eu NPs. For instance, nanoparticles coated by SEI detection antibodies are used to detect the toxin SEH thanks to a strip designed to capture the toxin SEG. Experiments are carried out for a toxin concentration of 5 ng.mL<sup>-1</sup>, that is the highest concentration used in this work for the non-multiplexed LFA. Images are quantitatively analyzed, the signal being defined as the ratio of the test line amplitude over the background. For the majority of the tested combinations, the signals are found to be lower than the LOBs determined in the standard configuration (e.g. SEH/SEH/SEH) with the same batch of strips (Table S11, left part, data in green). The only case of minor cross-talk appears when SEG capture antibodies are in the presence of the SEH toxin (Table S11, left part, data in red). Indeed, in the latter case, the non-specific signal represents 15 to 20 % of the signal obtained with the SEG/SEG/SEG system (Table S11, right part).

|                  |       | Test / Background<br>( [toxin] = 5 ng.mL <sup>-1</sup> ) |      |      | Percentage of the signal in the<br>standard (non-crossed) configuration |       |       |
|------------------|-------|--|------|------|---|-------|-------|
|                  |       | Eu NPs labelled by detection antibodies                  |      |      |   |       |       |
| Capture antibody | Toxin | SEG  | SEH  | SEI  | SEG   | SEH   | SEI   |
| SEG              | SEG   | 1.28   | 0.09 | 0.10 | 100.0   | 6.6   | 7.8   |
|                  | SEH   | 0.27   | 0.19 | 0.21 | 20.7  | 14.9  | 16.1  |
|                  | SEI   | 0.07   | 0.13 | 0.10 | 5.7   | 10.4  | 7.5   |
| SEH              | SEG   | 0.04   | 0.10 | 0.08 | 5.4   | 13.4  | 10.9  |
|                  | SEH   | 0.02   | 0.71 | 0.04 | 2.7   | 100.0 | 5.9   |
|                  | SEI   | 0.03   | 0.10 | 0.02 | 4.0   | 13.9  | 2.9   |
| SEI              | SEG   | 0.11   | 0.06 | 0.11 | 10.5  | 5.5   | 10.3  |
|                  | SEH   | 0.09   | 0.07 | 0.01 | 8.7   | 7.0   | 0.8   |
|                  | SEI   | 0.08   | 0.07 | 1.06 | 7.1   | 7.0   | 100.0 |

Table S11: Quantitative analysis of “test line / toxin / Eu Nps” combinations performed at 5 ng.mL<sup>-1</sup> of toxin, the green and the red colours corresponding to signals being respectively lower and higher than the LOB (left part). The results are also displayed in percentages of the non-crossed combinations (right part).

Assuming that the percentage of cross-reactivity is independent of the toxin concentration, we can estimate the signal for all the “SEX/SEY/SEZ” combinations carried out for toxin concentrations of 0.5 ng.mL<sup>-1</sup>. For this intermediate concentration, cross-talked signals are always found to be lower than the LOBs of the standard configuration. Even for the SEG test line and the SEH toxin combinations, the signal arising from cross-reactivity is 2 times lower than the LOB of the SEG/SEG/SEG configuration. Thus, the cross-reactivity at low toxin concentrations appears negligible, implying that there is no counter-indication for multiplexing LFA.

## S12 – Quantitative analysis of multiplexed strips labeled with Eu nanoparticles

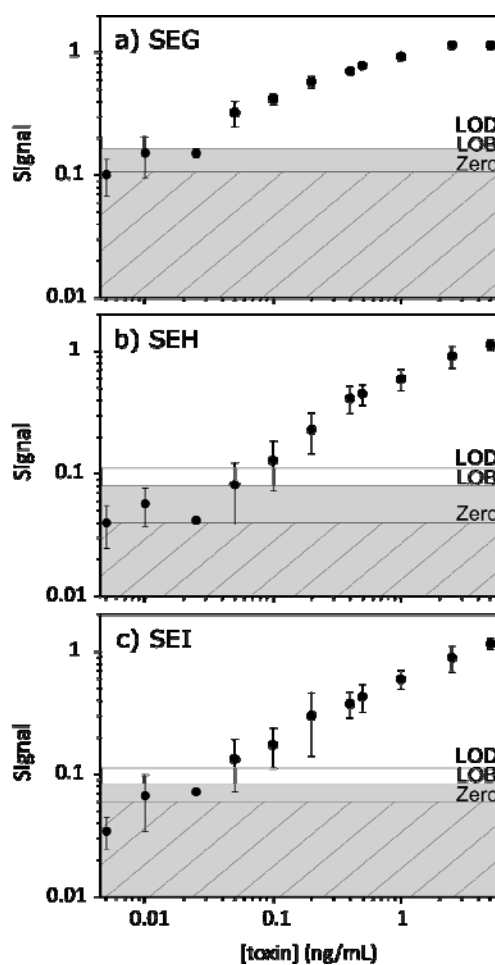


Figure S12: Quantitative analysis of SEG (a), SEH (b), and SEI (c) toxins performed in independent duplicates with Eu-doped NPs as probes for samples with identical SEG, SEH, and SEI concentrations. Error bars indicate the standard deviation of the two replicates. LOBs are determined at 0.02, 0.03, and 0.01 ng.mL<sup>-1</sup> for SEG, SEH, and SEI respectively from 8 independent zeros.

| [toxin]<br>(ng/mL) | SEG | SEH  | SEI |
|--------------------|-----|------|-----|
| 0                  | 7.5 | 11.3 | 8.5 |
| 0.005              | 1.3 | 3.4  | 3.7 |
| 0.01               | 1.6 | 3.1  | 4.9 |
| 0.025              | 1.4 | 1.1  | 2.8 |
| 0.05               | 2.8 | 1.2  | 2.9 |
| 0.1                | 2.2 | 1.0  | 2.1 |
| 0.2                | 1.8 | 1.0  | 2.0 |
| 0.4                | 1.4 | 1.1  | 1.4 |
| 0.5                | 1.3 | 1.0  | 1.3 |
| 1                  | 1.1 | 0.9  | 1.2 |
| 2.5                | 1.0 | 1.0  | 1.1 |
| 5                  | 0.9 | 1.1  | 1.2 |

Table S12: Ratio between  $C_{exp}$  and  $C_{nom}$  where  $C_{exp}$  are the concentrations obtained from the experimental multiplexed signal via the calibration curves determined with the simplex assays and  $C_{nom}$  are the nominal concentrations of SEG, SEH, and SEI simultaneously spiked in samples. The values in grey boxes correspond to the ratio calculated for toxin concentrations below the LOBs. The ratios for all the other values are found respectively between 0.9-2.8, 0.9-1.2, and 1.1-2.9 for SEG, SEH, and SEI.

S13 – Multiplexed strips with different toxin concentrations

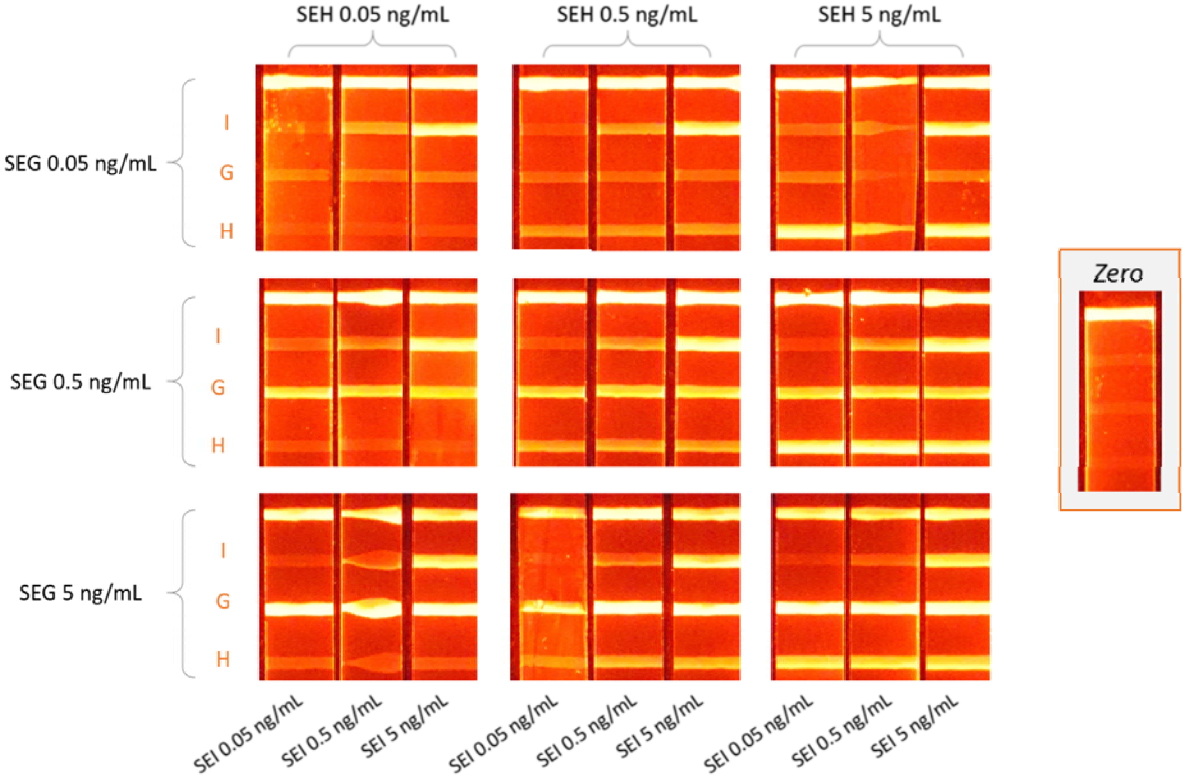


Figure S13: Combinatorial investigation of xLFA strips for SEG, SEH, and SEI concentrations at 0.05, 0.5, and 5 ng.mL<sup>-1</sup>. Insert: "zero" strip, i.e. with no toxin present in the analysed sample.

## References

1. Féraudet Tarrisse, C. *et al.* Highly sensitive and specific detection of staphylococcal enterotoxins SEA, SEG, SEH and SEI by immunoassay. *Toxins* **13**, 130 (2021).
2. Huignard, A., Gacoin, T. & Boilot, J.-P. Synthesis and Luminescence Properties of Colloidal  $\text{YVO}_4:\text{Eu}$  Phosphors. *Chem. Mater.* **12**, 1090–1094 (2000).
3. Casanova, D. *et al.* Counting the Number of Proteins Coupled to Single Nanoparticles. *J. Am. Chem. Soc.* **129**, 12592–12593 (2007).
4. Giaume, D. *et al.* Organic Functionalization of Luminescent Oxide Nanoparticles toward Their Application As Biological Probes. *Langmuir* **24**, 11018–11026 (2008).
5. Haiss, W., Thanh, N. T. K., Aveyard, J. & Fernig, D. G. Determination of Size and Concentration of Gold Nanoparticles from UV–Vis Spectra. *Anal. Chem.* **79**, 4215–4221 (2007).
6. Kittel, C. Introduction to Solid State Physics. 12.
7. Fleury, B. *et al.* Amorphous to Crystal Conversion as a Mechanism Governing the Structure of Luminescent  $\text{YVO}_4:\text{Eu}$  Nanoparticles. *ACS Nano* **8**, 2602–2608 (2014).
8. Casanova, D. *et al.* Optical *in situ* size determination of single lanthanide-ion doped oxide nanoparticles. *Appl. Phys. Lett.* **89**, 253103 (2006).
9. Würth, C., Grabolle, M., Pauli, J., Spieles, M. & Resch-Genger, U. Comparison of Methods and Achievable Uncertainties for the Relative and Absolute Measurement of Photoluminescence Quantum Yields. *Anal. Chem.* **83**, 3431–3439 (2011).
10. de Puig, H., Bosch, I., Gehrke, L. & Hamad-Schifferli, K. Challenges of the Nano–Bio Interface in Lateral Flow and Dipstick Immunoassays. *Trends in Biotechnology* **35**, 1169–1180 (2017).